Journal of Catalysis 274 (2010) 176–191

Contents lists available at ScienceDirect

Journal of Catalysis

journal homepage: www.elsevier.com/locate/jcat

Catalyst performance changes induced by palladium phase transformation in the hydrogenation of benzonitrile

Jasper J.W. Bakker [a,*], Anne Geert van der Neut [a], Michiel T. Kreutzer [b], Jacob A. Moulijn [a], Freek Kapteijn [a]

[a] Catalysis Engineering, Department of Chemical Engineering, Delft University of Technology, Julianalaan 136, 2628 BL Delft, The Netherlands
[b] Product and Process Engineering, Department of Chemical Engineering, Delft University of Technology, Julianalaan 136, 2628 BL Delft, The Netherlands

ARTICLE INFO

Article history:
Received 18 April 2010
Revised 20 June 2010
Accepted 26 June 2010
Available online 31 July 2010

Keywords:
Palladium
Palladium β-hydride
Benzylamine
Benzonitrile
Toluene
Selective hydrogenation
Hydrogenolysis
Condensation
Adsorption modes
Surface intermediates

ABSTRACT

The influence of hydrogen pressure on the performance of a γ-alumina-supported palladium catalyst was studied for the multiphase selective hydrogenation of benzonitrile to benzylamine and byproducts. Semi-batch experiments of benzonitrile hydrogenation in 2-propanol were performed with hydrogen pressures between 2.5 and 30 bar, at a constant temperature of 80 °C. The intrinsic property of palladium to absorb hydrogen into its lattice structure has a strong influence on activity and selectivity. The transformation to stable palladium β-hydride above a threshold hydrogen pressure of 10 bar induces a persistent change in turnover frequency and byproduct selectivity. The turnover frequency increases from 0.32 s^{-1} to a maximum of 0.75 s^{-1} at this threshold pressure and decreases to 0.25 s^{-1} with increasing hydrogen pressure. The palladium β-hydride phase suppresses the hydrogenolysis to toluene changing the selectivity from 6.5% to 2.0% and increasing the selectivity of the condensation to dibenzylamine from 1.6% to 2.7%, attributed to modified electronic interactions between catalyst and substrates. The selectivity to the desired product benzylamine is always high and increases with hydrogen pressure from 92.7% to 95.3%. The palladium catalyst state is mainly determined by the activation or operational hydrogen pressure, whichever was the highest, if the activation pressure was above 10 bar.

1. Introduction

The topic of this paper is structure sensitivity of palladium (Pd) catalysts, in particular the effect of structural changes due to Pd β-hydride (β-PdH) formation at higher hydrogen pressure (pH_2). The reaction of interest is the hydrogenation of aromatic nitriles to the corresponding primary amines. Here, controlling the selectivity is a crucial demand and insight into the reaction mechanisms of desired and undesired reactions is very valuable.

Primary aromatic amines are important chemical compounds that have found widespread applications as chemical and pharmaceutical intermediates, solvents, paints, herbicides and synthetic textiles. A major route to produce primary aromatic amines is the heterogeneously catalyzed hydrogenation of aromatic nitriles [1–4]. However, during the hydrogenation of aromatic nitriles toward the aromatic amines, several byproducts are usually formed, resulting in a loss of yield [1–4]. Activity and selectivity are mainly determined by the amount, type and mobility of surface intermediates and transition states which are controlled by the catalyst. Further, it should be noted that the reactant concentration, type of solvent(s), reaction conditions and additives (*e.g.* ammonia) also play an important role [2–4].

A scheme that depicts the reaction pathways during the hydrogenation of benzonitrile (BN) to benzylamine (BA) and the main byproducts can be found in Fig. 1. The reaction network is a combination of hydrogenation, condensation and hydrogenolysis reactions that can yield BA, *N*-benzylidenebenzylamine (DBI), dibenzylamine (DBA), and toluene (TOL), respectively. Ammonia (NH_3) is formed during condensation reactions and hydrogenolysis to TOL. The reaction mechanism is generally explained by the premise of benzylideneimine (BI) or other semi-hydrogenated intermediates and a surface aminal (*i.e.* α-aminodialkylamine (BIBA)).

Several authors contributed to the elucidation of the reaction mechanism since the beginning of the 20th century by proposing that imines (—CH=NH), Schiff bases (—C=N—C), and enamines (—N—C=C—) are the intermediates in the formation of primary, secondary, and tertiary amines [5–10]. However, this mechanism is based on a number of unproven assumptions that are corroborated only by indirect evidence: *e.g.* Schiff bases have been identified in solution, imines were detected on the catalyst surface by IR spectroscopy, and the absence of tertiary amine formation in the hydrogenation of BN has been observed. The inability to detect imine and enamine intermediates is attributed to their high reactivity.

* Corresponding author. Fax: +31 (0) 152785006.
E-mail address: j.j.w.bakker@tudelft.nl (J.J.W. Bakker).

0021-9517/$ - see front matter © 2010 Elsevier Inc. All rights reserved.
doi:10.1016/j.jcat.2010.06.013

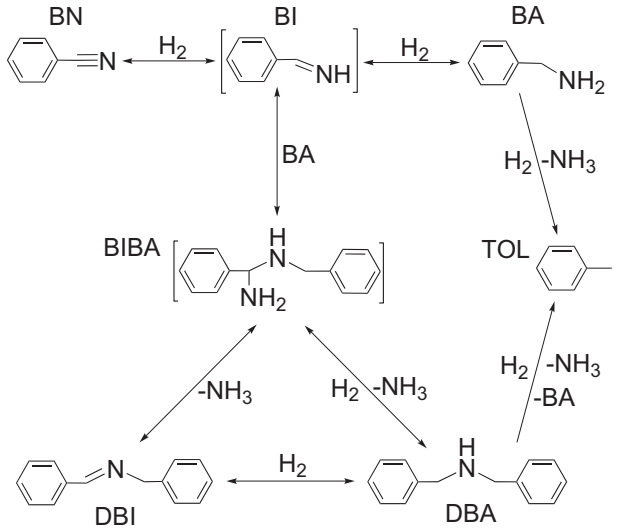

Fig. 1. Reaction pathways to different products in the hydrogenation of benzonitrile (BN): hydrogenation of BN to benzylamine (BA) via benzylideneimine (BI). Condensation of BA and BI via α-aminodialkylamine (BIBA) and *N*-benzylidenebenzylamine (DBI) to dibenzylamine (DBA). Hydrogenolysis to toluene (TOL) of DBA and BA. Direct hydrogenolysis of BIBA to DBA is possible. Species in between straight brackets are surface intermediates never detected in solution.

From several BN hydrogenation studies and our own findings, it can be concluded that the use of supported Pd catalysts results in high activity and, more important, a high selectivity toward BA compared to other platinum-group metal catalysts [11–15]. An overview of different catalysts used under many different conditions in the heterogeneous hydrogenation of BN is shown in Table 1. From our own investigations, it appeared that a commercially available γ-Al_2O_3-supported Pd catalyst exhibited the highest selectivity and was therefore used in this study.

While studying the effect of pH_2 on activity and selectivity over this catalyst, we encountered an unexpected anomaly: we found a maximum in catalyst activity with increasing pH_2, accompanied by a sudden selectivity shift in byproducts leading to an increased yield of BA. The literature does not report such an effect during Pd-catalyzed nitrile hydrogenation. However, in the hydrogenation and hydrogenolysis of hydroxymatairesinol using a Pd catalyst, Bernas et al. also encountered a negative dependence on the pH_2 above a certain pressure [16]. They explained this effect as a result of competitive adsorption of H_2 and the reactant. Dubois et al. studied the hydrogenation combined with hydrogenolysis of 2-methyl-2-nitropropane over a supported Pd catalyst and also encountered an activity maximum; they gave two possible explanations for this effect: more favorable H_2 adsorption for the same active sites or the formation of a new, less active, Pd phase [17]. Skakunova et al. hypothesized that the negative-order effect in the hydrogenolysis of propane over a Pd–Ru catalyst was caused by competitive adsorption of H_2 [18]. In general, hydrogenolysis reactions catalyzed by different supported metals are structure sensitive and often have a negative reaction order with respect to pH_2 up to −2.5 [19–23].

We demonstrate that in BN hydrogenation, competitive adsorption between H_2 and BN is not the explanation of the anomaly observed. Rather, our hypothesis is that structural changes of the Pd crystallites at higher pH_2 explain the observed phenomena. A well-known property of Pd, discovered by Graham in 1866 [24] that differentiates it from all other metals, is the easy absorption of atomic hydrogen in large quantities in the Pd lattice, occupying the octahedral interstices of its face-centered cubic Pd lattice structure already at ambient temperature and low pH_2 [25–27]. Upon absorbing large amounts of hydrogen, the lattice Pd expands (lattice constant increases) when the solid solution phase (α-PdH) transforms into the β-PdH phase [28]. Moreover, the character of the electronic *d*-band of Pd changes [27,29–32]. The amount of H absorption in Pd depends on the H_2 concentration in the liquid, temperature, Pd particle size, surface topography, support interactions, precursor, and pretreatment steps [28,33,34]. Structural changes upon transformation to β-PdH can have a profound effect on the adsorption strength, type, and amount of surface species, and thus on the activity and selectivity [28,35–42].

In this paper, we demonstrate that in γ-Al_2O_3-supported Pd-catalyzed BN hydrogenation, the β-PdH phase formed at increased pH_2 is responsible for the activity and selectivity effects. The pH_2 and the entailing transformation to β-PdH have a profound influence on the catalyst performance. Further, based on analysis of the reaction mixture and characterization of fresh, activated, and spent catalysts, a scheme of the reaction mechanism, modes of surface adsorption, and surface intermediates are presented. By combining *d*-band theory with simple frontier molecular orbital theory, we explain the observed results.

2. Experimental

2.1. Catalyst and materials

Unless explicitly stated, the experiments were carried out using reduced 5 wt% Pd/γ-Al_2O_3 supplied by Alfa Aesar. Blank experiments were performed using γ-Al_2O_3 (99.97%) supplied by Alfa Aesar. The catalysts we studied and reported in Table 1 (5 wt% Pd/C, 5 wt% Pd/$BaCO_3$, 5 wt% Ru/γ-Al_2O_3, 5 wt% Pt/C) were supplied by Aldrich. The other chemicals used in this study were purchased from commercial suppliers and used as received (benzonitrile, 99%, Alfa Aesar; benzylamine, >98%, Alfa Aesar; dibenzylamine, 98%, Alfa Aesar; toluene, 99.5%, J.T. Baker; *n*-isopropylbenzylamine, 98%, Alfa Aesar; 2-propanol, 99%, Aldrich; γ-Al_2O_3, 99.97%, Alfa Aesar).

2.2. Selective hydrogenation

The selective hydrogenation experiments were carried out in a semi-batch mode in a high-pressure stainless steel autoclave (Medimex Reactor CH-2543) equipped with baffles and a gas-induced stirrer. H_2 was continuously fed to the reactor to maintain a constant pH_2 (units: bar gauge further denoted as bar) during a hydrogenation experiment. We used a simple alcoholic solvent, 2-propanol, and did not use any additives.

In a typical experiment, 0.5 g of 5 wt% Pd/γ-Al_2O_3 was added to 150 ml of 2-propanol and subsequently fed to the reactor. Different cycles of pressurizing and depressurizing with N_2 were applied to remove the air from the reactor. Before a hydrogenation experiment, the catalyst was activated in the reactor in 2-propanol under elevated pH_2 at 80 °C for 1 h. The typical pH_2 used for the standard activation was 10 bar. In addition, the influence of activation pH_2 (2.5, 10, and 30 bar) on the catalyst performance was also investigated.

After the *in situ* activation of the catalyst, the reactor was brought to reaction conditions, *i.e.* a temperature (T) of 80 °C and a pH_2 between 2 and 30 bar for the different experiments. Then, 50 ml 2-propanol, adding up to 200 ml, with the appropriate amount of BN, was added to the autoclave via a pressurized filling tank ($C_{BN,0}$ = 520 mol/m^3). Reference hydrogenation experiments ($C_{BN,0}$ = 520 mol/m^3, T = 80 °C, pH_2 = 10 and 30 bar) were performed with a γ-Al_2O_3 support without Pd to determine its effect in the hydrogenation of BN. In addition, hydrogenation experiments with

Table 1
Hydrogenation of BN: comparison of BN conversion (X_{BN}), BA selectivity (S_{BA}), and yield (Y_{BA}) of different catalysts used in the literature and this study.

Catalyst	$C_{BN,0}$ (mol/m^3), solvent	T (°C), pH_2 (bar)	X_{BN} (%)	S_{BA} (%)	Y_{BA} (%)	Remarks	
5% Pt/C	–	100, 35	100	0	0	Pt: major product was DBA	[9,43]
5% Pd/C		100, 35	100	19	19		
5% Rh/C		100, 83	100	22	22	H_2O added	
5% Rh/C	2000, octane	25, 3.5	100	0	0	Mostly DBA was formed for Pt and Rh catalysts	[11–13]
5% Pt/C	2000, ethanol	25, 3.5	100	0	0		
5% Pd/C	2000, benzene	25, 3.5	100	63	63		
5% Pd/C	2000, hexane	25, 69	100	59	59	Adding diethylamine increased Y_{BA} to 100% for Pd catalysts	
5% Pd/C			100	34	34		
5% Ru/C			0	0	0		
5% Pt/C			38	7	18		
5% Pd/C			100	55	55		
5% Rh/C			100	33	33		
Raney Ni	485, methanol	100, 40	n.a.	76	n.a.	Several solvents used	[44]
2.5% Ir/Al_2O_3	220, ethanol	100, 21	20	n.a.	n.a.	Y_{DBA} was 36%	[45]
65% Ni/SiO_2/Al_2O_3	1000, methanol	120, 10	n.a.	n.a.	96	NH_3/CH_3OH added BN/NH_3 ratio = 2	[46]
60% Ni/SiO_2			n.a.	n.a.	99		
Pd/pyridyl	–	100, 36	100	26	26	32% TOL, 37% DBI	[47]
Raney Ni	1530, methanol	75, 40	88	91	80		
Ni–Mo (CH_2O)	485, methanol	105, 41	100	99	99	32% NH_3/H_2O added	[48,49]
10% Pd/C	323,	30, 6	95	95	90	NaH_2PO_4·H_2O added	[15]
5% Pd/C	H_2O/di-chloro-		95	94	89		
5% Pd/TiO_2	methane		71	94	67		
5% Pd/Al_2O_3			48	90	43		
Ni catalyst	n.a., ethanol	20, n.a.	100	61	61	Thiophene added	[50]
5% Pd/C	780,	85, 15	100	21	21	Higher S_{BA} achieved by adding NH_3	[14]
5% Pd/$BaSO_4$	2-propanol		100	24	24		
5% Pd/$CaCO_3$			100	15	15		
5% Pt/C			100	10	10		
Raney Ni			100	36	36		
Pt–Sn/nylon	192, ethanol	60, n.a.	100	15	15	Mostly DBA formed	[51]
Raney Ni		100, 15	100	95	95	Cont. counterc. reactor NH_3 accumulation	[52]
1% Pt/Al_2O_3	–	100, 7	99	0.1	0.1		
Sn–Pt/SiO_2	390, ethanol	60, 4	100	20	20	DBA major product	[53]
0.1% Pd/SiO_2	–	145, 8.3	46	n.a.	n.a.	Only X_{BN} reported	[54]
5% Pt/Al_2O_3	1000, methanol	100, 15	40	40	16	Dibenzylhydrazine	[55]
5% Pd/Al_2O_3	520, 2-propanol	80, 10	50	94[a]	86[b]	Main product for Pt/C was DBA	This study
5% Pt/C			50	1[a]	3[b]		
5% Pd/C			50	81[a]	61[b]	Main byproduct for Pd catalysts was TOL	
5% Pd/$BaCO_3$			50	34[a]	29[b]		
5% Ru/Al_2O_3			0	0[a]	0[b]		

n.a. – not available.
[a] S_{BA} at X_{BN} = 50%.
[b] Y_{BA} is maximum BA yield.

BA or mixtures of BN and BA were performed to get more insight into the mechanism. Our results reported in Table 1 (bottom row) were achieved under standard hydrogenation conditions ($C_{BN,0}$ = 520 mol/m^3, T = 80 °C, pH_2 = 10 bar). The supported Pd catalysts were activated for 1 h *in situ* in 2-propanol at 10 bar and 80 °C. The supported Pt and Ru catalysts were activated under H_2 flow for 1 h *ex situ* at 350 and 250 °C, respectively.

Samples were withdrawn from the reaction mixture during an experiment at selected intervals to determine the composition of the reaction mixture. Analysis of these samples was performed on a Chrompack CP9001 gas chromatograph equipped with FID detector and Chrompack Liquid Sampler 9050 autosampler fitted with a CP-SIL 8 column (length 50 m, 0.25 mm ID). The GC temperature program ranged from 50 to 250 °C at a heating rate of 10 °C/min. The standard deviation of the integrated peaks of the FID signal of the GC was 2.5%. GC data were checked by comparing H_2 flow into the autoclave with H_2 consumption as calculated on the basis of reaction stoichiometry and GC data. A normalized carbon balance was performed to check whether no other compounds were formed undetected by the GC analysis. The standard deviation of the balance was 2.4%.

No external and internal mass transfer limitations disguised our rate data. See Supplementary material for the details about the measurements and calculations performed.

Density functional theory (DFT) calculations were executed using the Becke 3LYP 6-31G* method to calculate the frontier orbital energy levels of the highest occupied molecular orbital (HOMO) and of the lowest unoccupied molecular orbital (LUMO) of the compounds involved in the hydrogenation of BN. These calculations were performed with the Spartan'06 package version 1.1.2 (a program for quantum mechanical computations) from Wavefunction, Inc. (http://www.wavefun.com).

The initial rate of consumption of BN is given as a turnover frequency (*TOF*) and is defined as

$$TOF = \frac{r}{\rho_{sites} \cdot a_{Pd}} \cdot N_A \quad (1)$$

where a_{Pd} is the specific surface area of Pd in m^2/g$_{Pd}$ as determined by CO chemisorption, ρ_{sites} is the site density of Pd in sites/m^2, N_A is the number of Avogadro in mol^{-1}, and r is the catalyst activity in mol/g$_{Pd}$/s and is defined as

$$r = \frac{dC_{BN}}{dt} \cdot \frac{1}{W_{Pd}} \quad (2)$$

where W_{Pd} is the concentration of Pd per liquid volume in g_{Pd}/m^3_{liquid}. The activity is determined at the start of a hydrogenation experiment up to 10% conversion of BN.

The conversion of BN (X_{BN}) is defined as

$$X_{BN} = \frac{C_{BN,0} - C_{BN}}{C_{BN,0}} \times 100\% \quad (3)$$

where $C_{BN,0}$ is the concentration of BN at $t = 0$ min and C_{BN} the actual concentration of BN both in mol/m^3.

All selectivities (S_x) are determined at $X_{BN} = 50\%$ and are defined as

$$S_x = \frac{C_x}{C_{BN,0}} - C_{BN} \times 100\% \quad (4)$$

where x is BA, TOL, or DBA.

The desired product is BA and the maximum yield of BA (Y_{BA}) is defined as

$$Y_{BA} = \frac{C_{BA,max}}{C_{BN,0}} \times 100\% \quad (5)$$

where $C_{BA,max}$ is the maximum concentration of BA in mol/m^3.

The TOL yield (Y_{TOL}) and DBA yield (Y_{DBA}) are defined as $C_{TOL}/C_{BN,0}$ and $C_{DBA}/C_{BN,0}$, respectively, at Y_{BA}.

2.3. Catalyst characterization

Prior to analysis, fresh, activated, and spent catalyst samples were dried in an oven (static air atmosphere) that was ramped up from room temperature at a heating rate of 0.5 °C/min up to 120 °C, followed by 2 h at 120 °C.

The catalysts were characterized using X-ray powder diffraction (XRD), temperature-programmed reduction (TPR), thermal gravimetric analysis (TGA), inductively coupled plasma optical emission spectroscopy (ICP-OES), diffuse reflectance infrared Fourier transform (DRIFT), CO chemisorption, N_2 physisorption, transmission electron microscopy (TEM), and laser diffraction. The details regarding these characterization methods can be found in the Supplementary material. Note that XRD and TPR were only performed on fresh and activated Pd/γ-Al_2O_3 catalysts. To obtain references for TGA and DRIFT, fresh Pd/γ-Al_2O_3 catalyst was soaked in pure BN, BA, and DBA for 4 h at 80 °C. Fresh Pd/γ-Al_2O_3 catalysts were also investigated with TGA and DRIFT. Characterization of spent Pd/γ-Al_2O_3 catalysts using TGA and DRIFT was performed after hydrogenation experiments that were stopped at Y_{BA}. Characterization of spent Pd/γ-Al_2O_3 catalysts using ICP-OES, CO chemisorption, N_2 physisorption, TEM, and laser diffraction was performed after hydrogenation experiments stopped at $X_{BA} = 100\%$.

3. Results

3.1. Hydrogenation of benzonitrile

Typical concentration–time profiles of the various components involved in the semi-batch hydrogenation of benzonitrile (BN) using a Pd/γ-Al_2O_3 catalyst, activated at 10 bar, at 80 °C with a pH_2 of 5.3 and 15 bar are shown in Fig. 2a and b. Fig. 2a also shows where the catalyst performance parameters, *i.e.*, turnover frequencies, selectivities, and yields, were determined in the concentration–time profiles by using formulas (1)–(5) defined in the experimental part. Concentration–time profiles of the hydrogenation of BA ($C_{BA,0} = 520$ mol/m^3) and of a mixture of equimolar amounts of BN and BA ($C_{BN,0} = C_{BA,0} = 300$ mol/m^3) performed at $pH_2 = 10$ bar and $T = 80$ °C (standard activation procedure used) are shown in Fig. 2c.

The main product is benzylamine (BA) at the investigated pH_2 range. The major byproducts are toluene (TOL) and dibenzylamine (DBA). Together with BN, these three compounds make up more than 99% of the carbon mass balance. We did not find half-hydrogenated species, *e.g.* benzylideneimine (BI) or *N*-benzylidenebenzylamine (DBI), in the reaction mixture. Also, no DBI was found in solution, which is supposed to be a relatively stable imine [56] and has been detected by several researchers in the hydrogenation of BN [57]. A minor byproduct detected was *N*-isopropylbenzylamine (<1%) which is a product of the reaction between BA and the solvent (2-propanol).

The initial concentration–time profile of DBA in Fig. 2a is an *s*-shaped curve, whereas the formation of TOL starts from $t = 0$ min onwards, and a straight line can be fitted through the data points. This is an indication that TOL is also formed from BN directly, via surface intermediates, without desorption and readsorption of BA. After the maximum in C_{BA} (*i.e.* Y_{BA}), when BN was mostly depleted, hydrogenolysis of BA to TOL takes off (Fig. 2). The rate of TOL formation and BA depletion are equal after full conversion of BN.

*TOF*s, selectivities, and yield versus pH_2 are given in Fig. 3. The standard condition is $C_{BN,0} = 520$ mol/m^3, but also experiments were conducted at $C_{BN,0} = 300$ and 1000 mol/m^3, see Fig. 3a. Clearly, for these experiments, the *TOF*s are the same as for the standard conditions.

Concentration–time profiles with variation of activation and hydrogenation pressure are shown in Fig. 4a and b. Fig. 4a shows two concentration–time profiles: one with activation at 10 bar followed by hydrogenation at 30 bar, and one with 30-bar activation followed by 10-bar hydrogenation. These two configurations give equal results. Fig. 4b shows three concentration–time profiles: 10-bar activation followed by 2.5-bar hydrogenation, 2.5-bar activation followed by 10-bar hydrogenation, and 10-bar activation followed by 10-bar hydrogenation. The activation at 2.5 bar followed by 10-bar hydrogenation displays similar results as 10-bar activation followed by 10-bar hydrogenation, but 10-bar activation followed by 2.5-bar hydrogenation yields different results. The results for 30-bar activation followed by 10-bar hydrogenation (Fig. 4a) and 10-bar activation followed by 10-bar hydrogenation (Fig. 4b) are also dissimilar from each other.

3.2. Catalyst characterization

An overview of the characterization of the fresh, activated, and spent Pd catalysts is shown in Table 2. ICP-OES analysis showed a Pd content of 4.22 wt% in the fresh catalyst. This value did not change during activation or hydrogenation at different pH_2, so, no leaching occurred during any of the activation steps or hydrogenation. The S_{BET} of the γ-Al_2O_3 support was 154 m^2/g with a pore volume of 0.47 cm^3/g and a mean pore diameter of 12 nm. The mean particle size of the γ-Al_2O_3 support was 37 μm and did not undergo any significant change during activation or hydrogenation.

The average size of the Pd crystallites of the fresh catalyst was 5.6 nm (dispersion = 20.0%) and 4.2 nm (dispersion = 26.7%) determined by CO chemisorption and TEM, respectively. The Pd crystallites were uniformly distributed over the γ-Al_2O_3 support. The discrepancy between the Pd crystallite sizes can be explained by the error we introduce by assuming that the CO/Pd ratio is unity in the calculation of the Pd crystallite size from CO chemisorption measurements. CO is known to adsorb on Pd not only in an end-on configuration (CO/Pd = 1) but also in a bridged configuration (CO/Pd = 0.5) [58–60]. After activation at 10 and 30 bar, no changes to the average Pd crystallite size was observed,

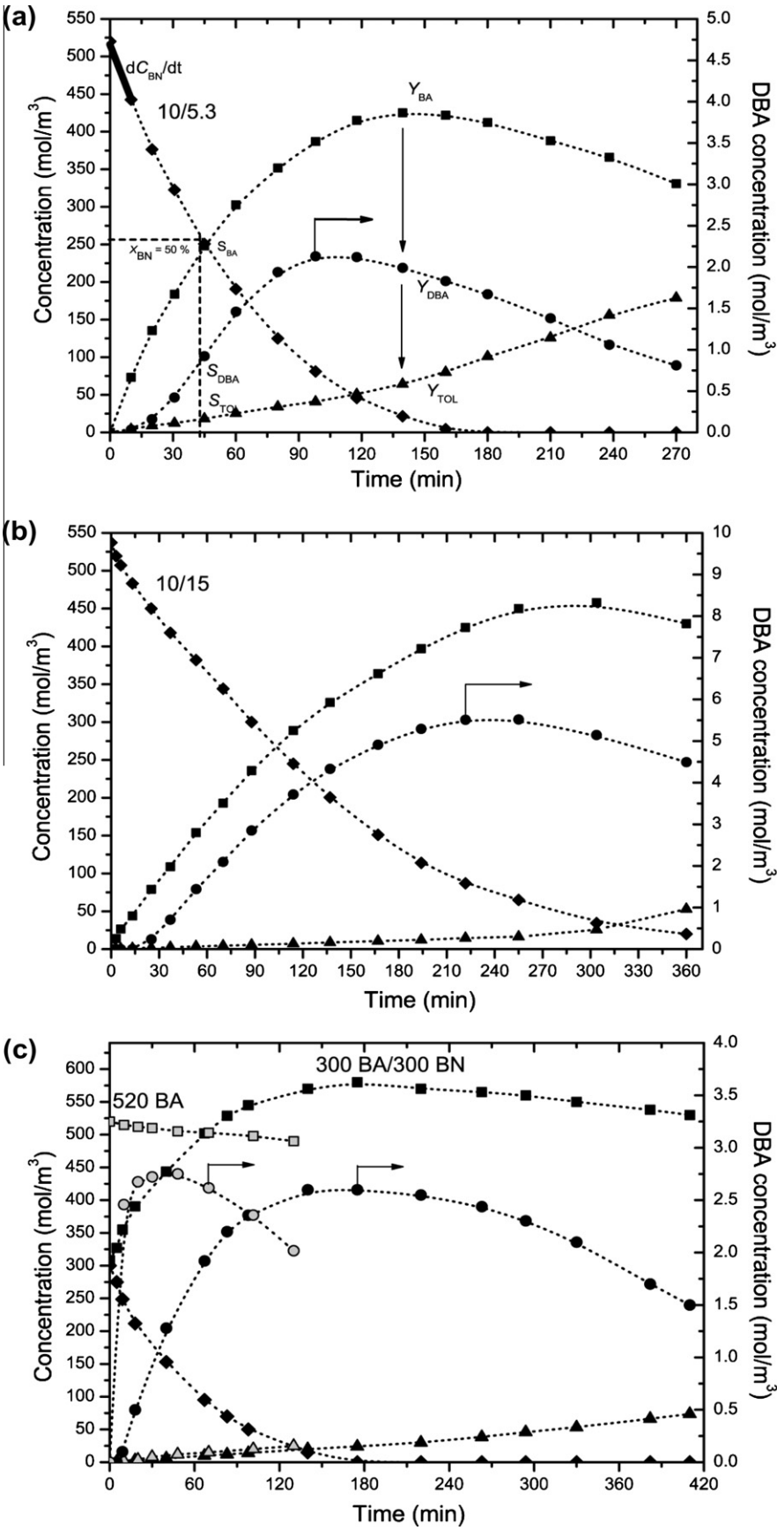

Fig. 2. Concentration (mol/m^3) vs. time (min) profiles for BN hydrogenation at 80 °C over a Pd/γ-Al_2O_3 catalyst with $C_{BN,0}$ = 520 mol/m^3 performed at 5.3 (a) and 15 (b) bar H_2; (c) concentration (mol/m^3) vs. time (min) profiles for BA hydrogenation with $C_{BA,0}$ = 520 mol/m^3 (gray symbols) and hydrogenation of a mixture of BN and BA with $C_{BN,0}$ = 300 mol/m^3 and $C_{BA,0}$ = 300 mol/m^3 (black symbols) at 80 °C over a Pd/γ-Al_2O_3 catalyst at 10-bar hydrogenation. All catalysts were activated at 10 bar. Left y-axis shows the concentration of BN, BA and TOL. The right y-axis shows the DBA concentration. Key: ♦ = C_{BN}; ■ = C_{BA}; ● = C_{DBA}; ▲ = C_{TOL}. The dashed lines are guidance for the eyes.

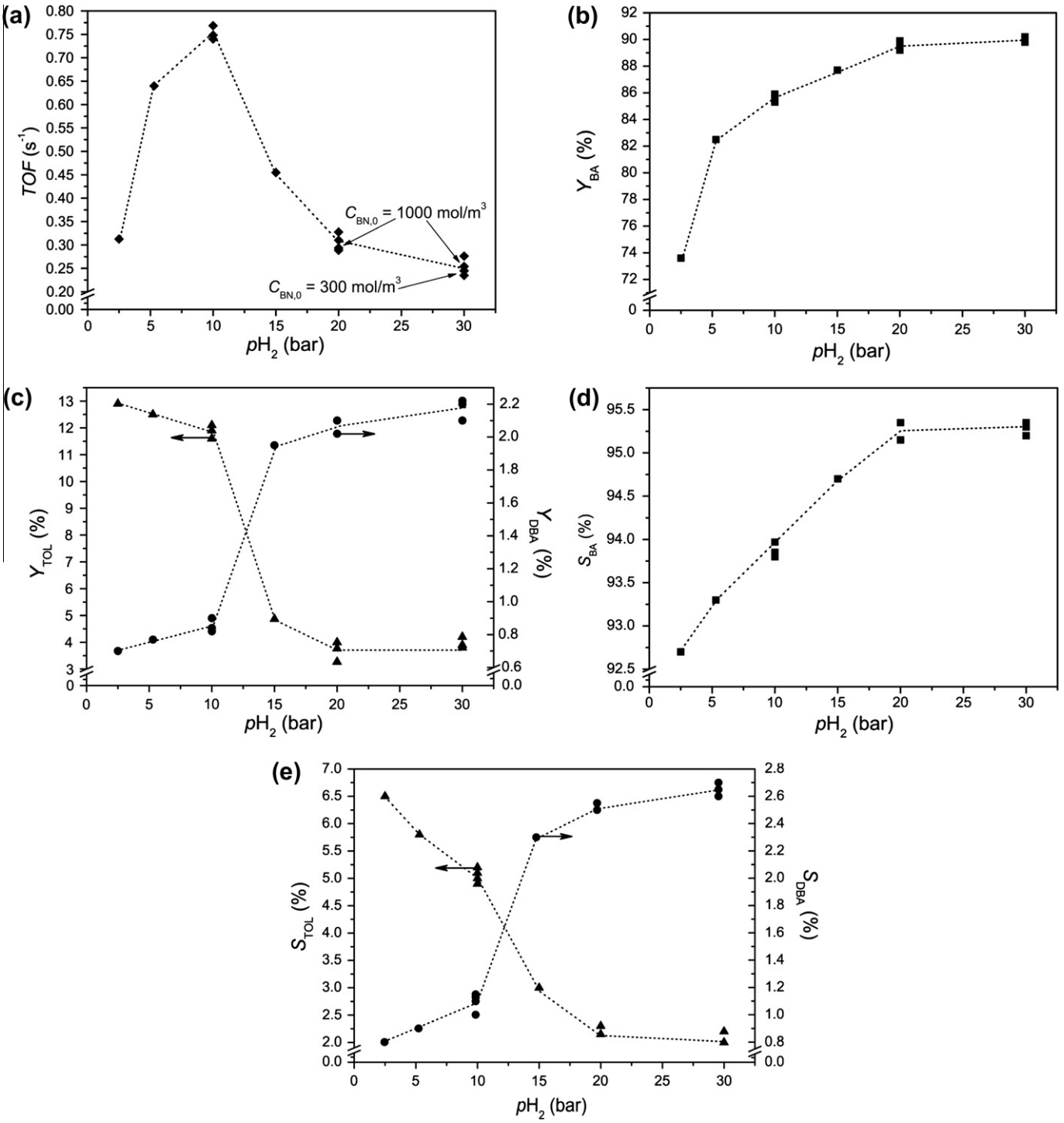

Fig. 3. Catalyst performance vs. pH_2 (bar) for BN hydrogenation over a Pd/γ-Al_2O_3 catalyst at 80 °C, $C_{BN,0}$ = 520 mol/m^3, and 10-bar activation: (a) turnover frequencies (*TOF*). The diamonds indicated by the arrows at 20 and 30 bar pH_2 represent hydrogenations performed at $C_{BN,0}$ = 1000 mol/m^3 and 300 mol/m^3; (b) maximum BA yield (Y_{BA}); (c) Y_{TOL} (left *y*-axis) and Y_{DBA} (right *y*-axis) at Y_{BA}; (d) S_{BA} at X_{BN} = 50%; (e) S_{TOL} (left *y*-axis) and S_{DBA} (right *y*-axis) at X_{BN} = 50%. Key: ♦ = *TOF*; ■ = S_{BA} or Y_{BA}; ● = S_{DBA} or Y_{DBA}; ▲ = S_{TOL} or Y_{TOL}. The dashed lines are guidance for the eyes.

whereas the spent catalysts (hydrogenations performed at 10 and 30 bar) showed an increase in the average Pd crystallite size from 5.6 to 6.2 nm. However, TEM analysis did not show any growth of the Pd crystallite size: the average Pd crystallite size of the fresh and spent catalyst was 4.2 nm. The increased average Pd crystallite size of the spent catalyst (*i.e.* lower Pd surface area) as measured with CO chemisorption is probably caused by adsorbed species on the Pd surface that decrease the area that is available for chemisorption of CO.

Ex situ X-ray diffraction patterns of four Pd/γ-Al_2O_3 catalysts activated at different pH_2 are shown in Fig. 5. The Pd(3 1 1) reflections region is presented because there is no interference of γ-Al_2O_3 support peaks in this region. Note that the Pd(1 1 1) reflection showed the same trends but was heavily obscured by γ-Al_2O_3 support reflections. The reflection at 2θ = 84.6° is a reflection of the crystalline part of the γ-Al_2O_3 support and is shown in Fig. 5 as a reference. The observed Bragg diffraction reflections correspond to Pd(3 1 1) and β-PdH_x(3 1 1) reflections.

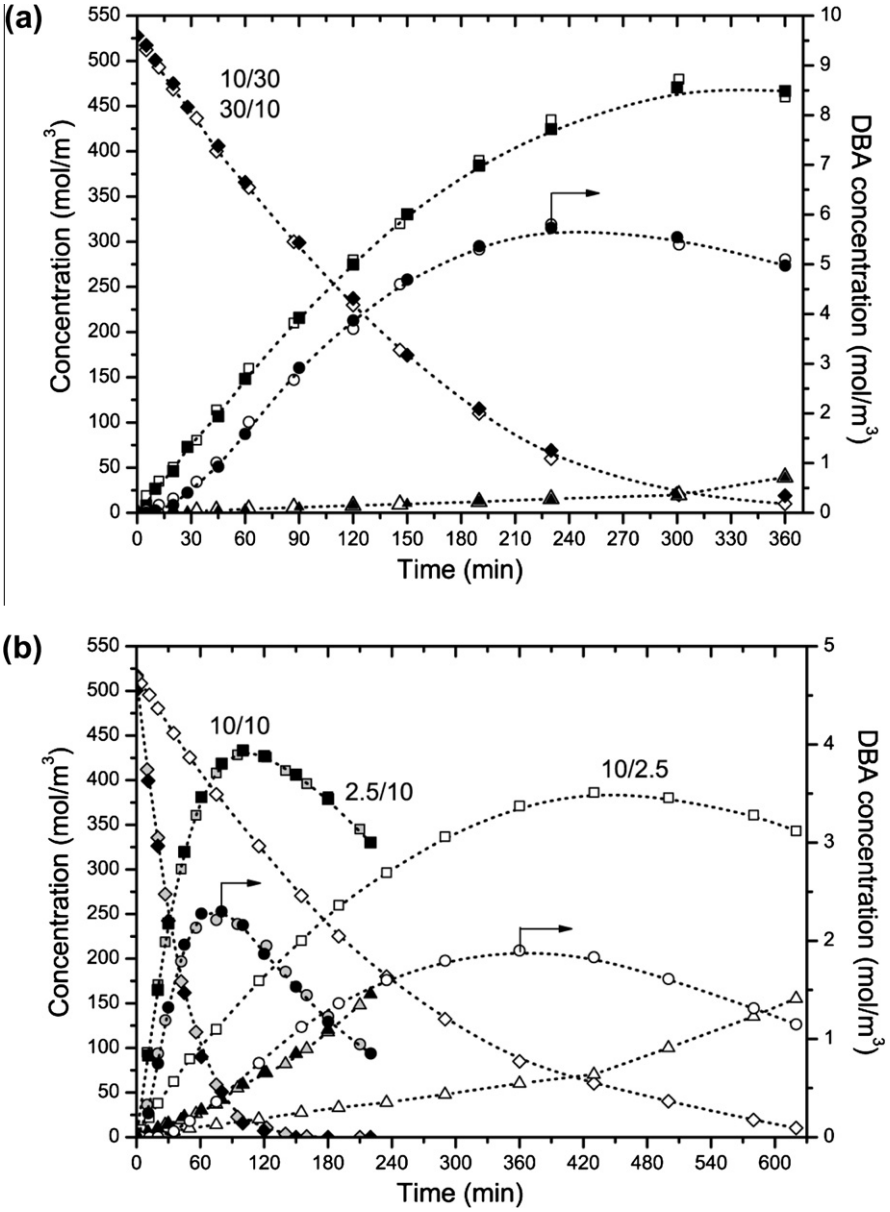

Fig. 4. Concentration (mol/m^3) vs. time (min) profiles of BN hydrogenation over a Pd/γ-Al_2O_3 catalyst at different activation and hydrogenation pressures at 80 °C and $C_{BA,0}$ = 520 mol/m^3: (a) 30-bar activation and 10-bar hydrogenation (open markers) and 10-bar activation and 30-bar hydrogenation (closed markers); (b) 10-bar activation and 10-bar hydrogenation (gray markers), 10-bar activation and 2.5-bar hydrogenation (open markers), and 2.5-bar activation and 10-bar hydrogenation (closed markers). Left *y*-axis shows the concentration of BN, BA, and TOL. The right *y*-axis shows the DBA concentration. Key: ♦ = C_{BN}; ■ = C_{BA}; ● = C_{DBA}; ▲ = C_{TOL}. The dashed lines are guidance for the eyes.

Table 2
Summary of characterization results of fresh, activated, and spent 5 wt% Pd/γ-Al_2O_3 catalyst.

Catalyst	Average Pd crystallite size (nm)		Pd loading (wt%)	S_{BET} (m^2/g)	D < 50%[a] (μm)
	CO chemisorption[b]	TEM	ICP-OES	N_2 physisorption	Laser diffraction
Fresh	5.6	4.2 ± 0.6	4.22	154	37
Activated at 10 bar	5.6	n.m.	4.22	n.m.	n.m.
Activated at 30 bar	5.6	n.m.	4.21	154	n.m.
Spent 10 bar	6.2	4.2 ± 0.9	4.23	n.m.	37
Spent 30 bar	6.2	n.m.	4.22	150	n.m.

n.m. – not measured.
[a] D < 50% is the diameter below which 50% of the particle volume is comprised.
[b] Assumptions: CO:Pd = 1 and spherically shaped crystallites.

When H_2 is absorbed in the Pd lattice structure and β-PdH is formed, the Bragg reflection shifts to smaller 2θ angles of around 79.7° (indicated with the arrow in Fig. 5) due to expansion of the Pd lattice. Reflections at 81.6° with a calculated lattice constant

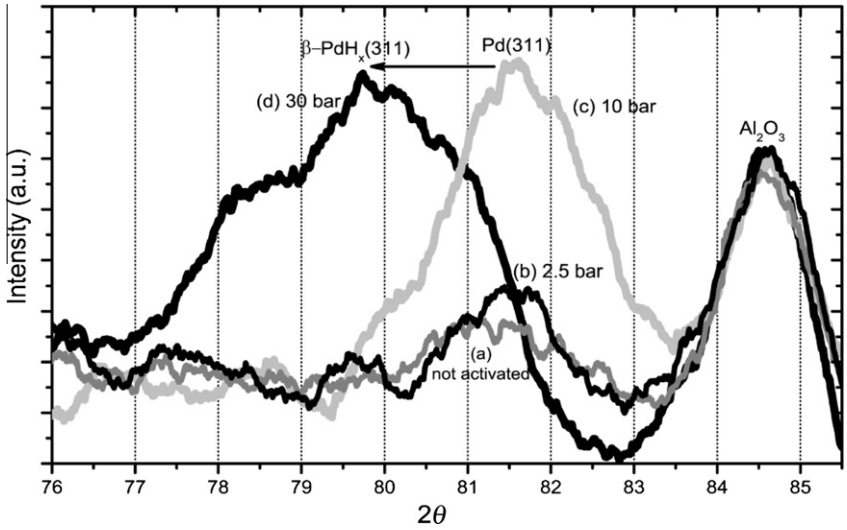

Fig. 5. Four ex situ X-ray diffraction patterns of Pd/γ-Al_2O_3 catalysts activated at different pH_2 at 80 °C in 2-propanol prior to XRD analysis. Key: (a) = not activated; (b) = activated at 2.5 bar; (c) = activated at 10 bar; (d) = activated at 30 bar.

of 3.91 Å and 79.7° with a calculated lattice constant of 3.99 Å are from Pd(3 1 1) and β-PdH$_x$(3 1 1), respectively. So, the lattice constant of Pd increases 2.0% when a pH_2 of 30 bar is applied during the activation step (in 2-propanol at 80 °C for 1 h). The amount of hydrogen absorbed (represented by x in β-PdH$_x$) in the Pd crystallites correlates with the location of the Bragg reflection and is determined by the Pd crystallite size: smaller Pd crystallites absorb less hydrogen in the β-PdH phase and more in the α-PdH phase [33,34,61]. We determined x for the -PdH phase using Vegard's law and lattice constants and x-values for similarly sized nanoscale particles from the literature as x = 0.43 [62]. The lattice constant for Pd(3 1 1) is reported to be 3.89 Å [63]. Compared to our lattice constant of 3.91 Å, it shows that the fresh catalyst and those activated at 2.5 and 10 bar experienced minor lattice expansion, obviously because of the pretreatment steps and x being 0.06. Note that the fresh catalyst had already been reduced by the supplier. The catalysts activated at 2.5 and 10 bar also showed a small reflection at 79.8° but the main reflection was from Pd(3 1 1) at 81.5°.

The catalyst activated at 10 and 30 bar showed a strong increase in intensity of the Pd(3 1 1) and β-PdH$_{0.43}$(3 1 1) reflections, respectively. Note that the 10-bar experiment did not shift the 3 1 1 reflection to smaller 2θ angles. The increase in intensity could be caused by a rise in the average length of an ordered row of atoms in the 3 1 1 crystallographic direction caused by structure rearrangement: exposure to H_2 can result in ordering of Pd crystallites [64]. Although XRD is considered as a bulk characterization technique, surface topography changes can also enhance the intensity of a reflection since for nanoscale particles a substantial amount of the atoms is located at the surface. The observed broadening of the β-PdH$_{0.43}$(3 1 1) reflection (Fig. 5) is attributed to microstrain (*e.g.* from non-uniform lattice distortion) and solid solution inhomogeneity.

Three H_2–TPR curves, two of Pd/γ-Al_2O_3 catalysts that were activated at 10 and 30 bar H_2 (in 2-propanol at 80 °C for 1 h) and a fresh Pd/γ-Al_2O_3 catalyst, are shown in Fig. 6. The H_2–TPR curves all have a negative H_2 peak around 83 °C, which is characteristic of Pd catalysts with Pd crystallite sizes larger than 2–3 nm. This peak is attributed to the H_2 desorption from the decomposition of the β-PdH$_x$ formed by the uptake of H_2 at room temperature (5 min) during the TPR experiment [65–68]. The area of the β-PdH$_x$ decomposition peak was determined in the temperature range 60–100 °C [60,69–72]. The β-PdH$_x$ decomposition peak area decreased by 20% and 28% (corrected by the weight of the samples) if the Pd/γ-Al_2O_3 prior to H_2–TPR was activated at 10 and 30 bar, respectively.

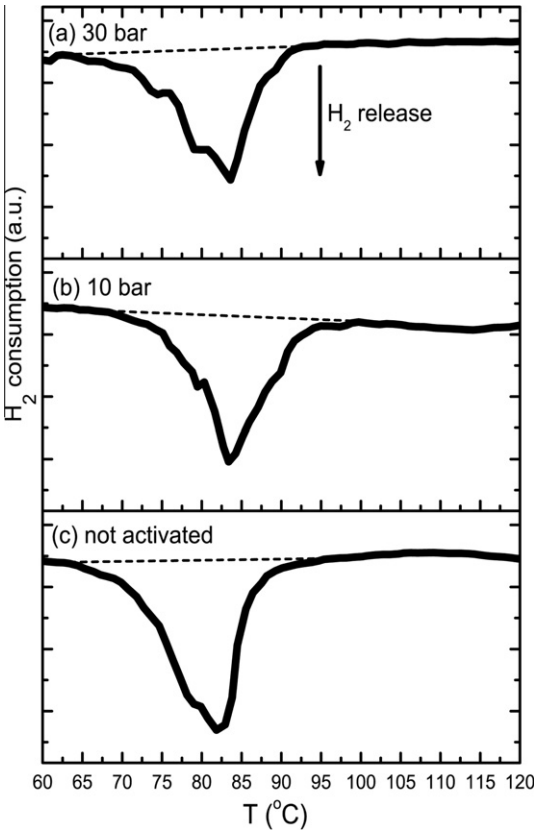

Fig. 6. H_2–TPR profiles of three Pd/γ-Al_2O_3 catalysts activated prior to H_2–TPR at different pH_2 in 2-propanol for 1 h at 80 °C. Key: (a) = 30-bar activation; (b) = 10-bar activation; (c) = not activated. The dashed lines show the baselines for the determination of the relative amounts of H_2 release.

The overall DRIFT spectra indicated that BA and BN were adsorbed in excess on the catalyst surface when comparing these spectra with reference spectra (not shown). An overall DRIFT spectrum of a spent Pd/γ-Al_2O_3 catalyst used in hydrogenation at 20 bar

is shown in Fig. 7a. The hydrogenations were stopped directly after Y_{BA} was reached. DRIFT spectra of the ν(C≡N) stretching region of two spent Pd/γ-Al_2O_3 catalysts from a 10- and 20-bar hydrogenation experiment are shown in Fig. 7b. The C≡N stretches are very valuable characteristics because they fall in a practically unpopulated spectral region [73]. A DRIFT spectrum of a fresh Pd/γ-Al_2O_3 catalyst did not show any peaks in this region (not shown). Free BN shows a band at 2231.7 cm^{-1} in 2-propanol [74]. Interactions of γ-Al_2O_3 surface groups (*e.g.* acidic Al_T^{3+} and Al_O^{3+}, basic and acidic Al—OH groups) with BN are found above 2240 cm^{-1} but most interactions of the acidic γ-Al_2O_3 groups will be with NH_3 and amine species [75–77]. The interaction at 2245 cm^{-1} is attributed to end-on adsorption via an acidic Al—OH of γ-Al_2O_3. Several configurations of BN adsorption are possible on Pd, *i.e.*, end-on and side-on. After hydrogenations at 10 and 20 bar, both adsorption configurations were observed (Fig. 7b): side-on adsorption at ~2165 cm^{-1} and end-on at ~2229 cm^{-1}. Strikingly, there is a distinct difference between the BN adsorption configuration ratios (side-on/end-on) for both spent catalysts: this ratio is much larger for hydrogenation at 10 bar than at 20 bar.

Thermogravimetric analyses of two spent Pd/γ-Al_2O_3 catalysts used in hydrogenations at 10 and 20 bar are compared in Fig. 8. It is also shown in Fig. 8 whether exothermic combustion or endothermic desorption occurred, as determined by single-point differential thermal analysis (STDA) present in the thermobalance. The total weight loss (discarding water and catalyst peaks) was 3.1 ± 0.1 and 4.3 ± 0.2 wt% for hydrogenations at 10 and 20 bar, respectively. The weight loss of 2 ± 0.1 wt% at 75 °C (endothermic) is due to desorption of physisorbed water. The weight loss at 190 and 215 °C (both exothermic) for the 10- and 20-bar experiment, respectively, originates from decomposition of adsorbed species. From reference experiments (not shown), it is concluded that this weight loss (at 190 and 215 °C) is from decomposition of BA. The catalyst used in hydrogenation at 20 bar showed more strongly adsorbed and larger amounts of BA on the catalyst surface: 0.7 ± 0.1 and 1.3 ± 0.1 wt% for hydrogenation at 10 and 20 bar, respectively. A weight loss of 0.8 ± 0.1 wt% at 260 °C (for hydrogenation at 10 and 20 bar) originates from desorption of the Pd precursor (endothermic), because this weight loss also occurred when TGA is performed using a fresh catalyst (not shown). The weight loss around 285 °C (exothermic) observed in the thermographs of both spent catalysts was not detected in the thermographs of a fresh catalyst and catalysts used in the reference experiments. This weight loss was ascribed to decomposing semi-hydrogenated species that were chemisorbed on the Pd crystallites. The weight losses at 340 and 440 °C (both exothermic) are from combustion of basic species (*e.g.* BA, DBA, and NH_3) deposited near Pd crystallites and on the γ-Al_2O_3 support, respectively [78–81]. A catalyst used in hydrogenation at 10 bar contains less of these deposits on the surface: 2.0 ± 0.1 and 3.0 ± 0.1 wt% for hydrogenation at 10 and 20 bar, respectively.

The weight loss at 810 °C (exothermic) is also seen in the TGA of a soaked catalyst in BN but was absent for the catalysts soaked in the other compounds. The weight losses were 0.4 ± 0.02 and 0.1 ± 0.01 wt% for the 10 and 20 bar experiment, respectively. The weight loss of 0.5 ± 0.02 wt% at 860 °C (exothermic) is from the phase transformation of γ-Al_2O_3 to δ-Al_2O_3 [82] and was also visible in the TGA of a fresh catalyst sample.

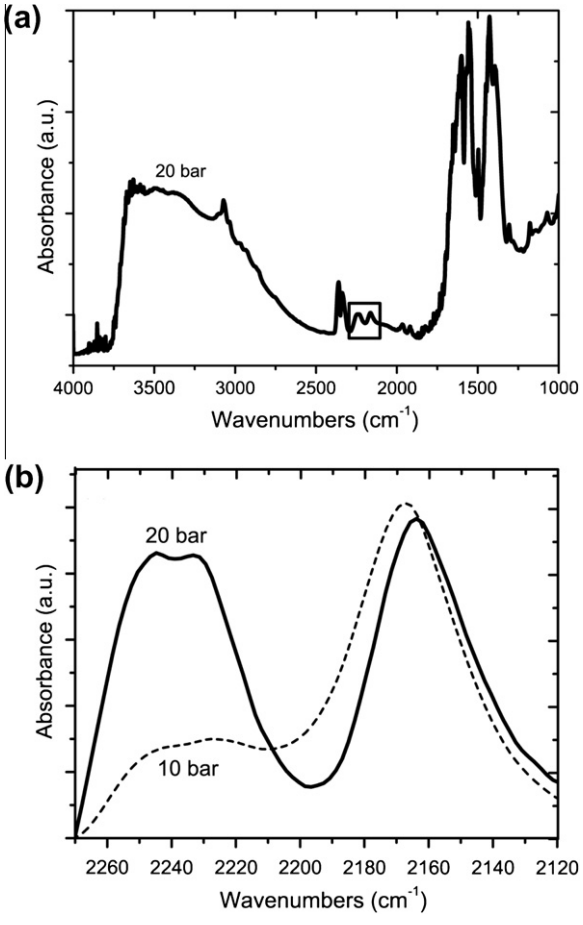

Fig. 7. DRIFT spectra of spent Pd/γ-Al_2O_3 catalysts after BN hydrogenations performed at 10 and 20 bar at 80 °C, $C_{BN,0}$ = 520 mol/m^3, and 10-bar activation. The reactions were stopped at Y_{BA}: (a) full spectrum for hydrogenation performed 20 bar showing the C≡N stretching region indicated by the square; (b) enlarged C≡N stretching region for hydrogenation performed at 10 (dashed line) and 20 bar (full line).

3.3. Molecular orbital energy calculations

The calculated values of HOMO and LUMO energy levels are shown in Table 3. The LUMO level represents the ease to accept electrons: the lower the LUMO the easier it accepts electrons. The lowest calculated LUMO level is the π C≡N orbital of BN at −1.41 eV. The HOMO level represents the ease to donate electrons: the higher the HOMO level the better it donates electrons. BIBA, DBA, and BA show the highest HOMO levels at −6.11, −6.09, and −6.18, respectively. Note that the orbital energy levels were calculated without any interaction with the Pd surface or solvent effects taken into account. The orbital levels for the intermediates are thereby speculative: first, because the intermediates were not observed during reaction and secondly, because interaction with the surface might significantly alter the levels of these short-lived intermediates.

4. Discussion

Some striking peculiarities related to the activity and selectivity of the hydrogenation of BN over Pd/γ-Al_2O_3 have been observed. Upon increasing pH_2, the activity of the catalyst goes through a maximum around 10 bar, while the product selectivities show a steep change around this pH_2. Moreover, the turnover frequency and selectivities depend on the activation pH_2 prior to hydrogenation.

4.1. Activity profile vs. pH_2

The *TOF* of BN hydrogenation increases with increasing pH_2, up to 10 bar, where it reached its maximum (Fig. 3a). Above the

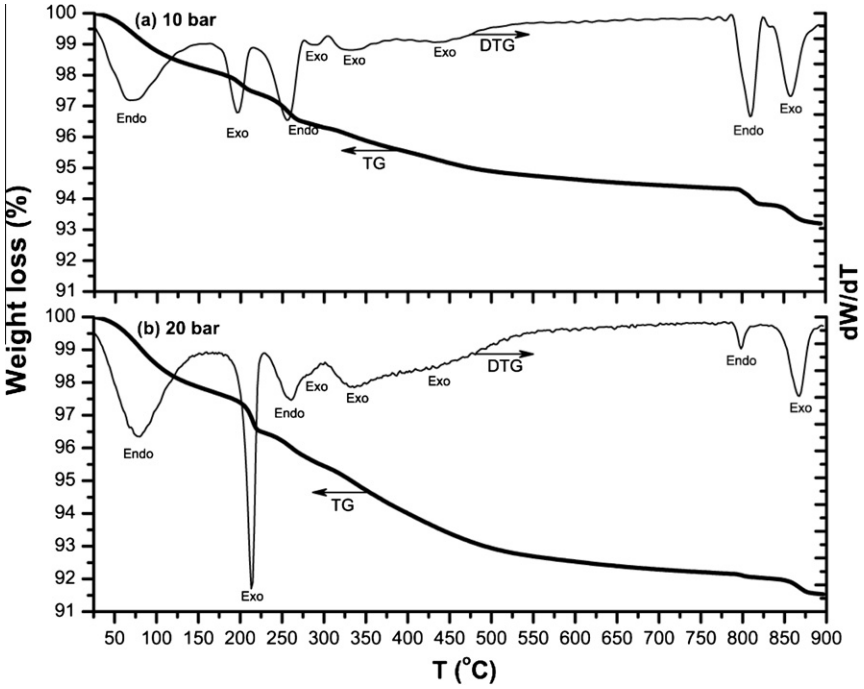

Fig. 8. Thermogravimetric (TG) and differential thermogravimetric (DTG) profiles in air of two spent Pd/γ-Al_2O_3 catalysts after hydrogenation performed at 10 bar (a) and 20 bar (b) at 80 °C, $C_{BN,0}$ = 520 mol/m^3, and activated at 10 bar. The reactions were stopped at Y_{BA}. The left *y*-axis represents the weight loss and the right *y*-axis represents the differential weight loss. Key: endo = endothermal desorption process; exo = exothermal decomposition process; as determined by the single-point differential thermal analysis (SDTA) present in the thermobalance.

Table 3
HOMO–LUMO levels.

Species	HOMO[a] (eV)	LUMO[b] (eV)
BN	−7.26	−1.41
BI (Z)	−6.61	−1.19
BI (E)	−6.84	−1.33
BA	−6.18	0.05
TOL	−6.40	0.14
NH3	−6.87	2.14
BIBA	−6.11	0.10
DBI (E)	−6.43	−1.18
DBI (Z)	−6.44	−1.07
DBA	−6.09	0.08
2-Propanol	−7.10	1.96

Calculated using Becke 3LYP 6-31G* method.
[a] HOMO = highest occupied molecular orbital.
[b] LUMO = lowest unoccupied molecular orbital.

threshold pH_2 of 10 bar, further increasing pH_2 showed a strong inverse effect on the reaction rates and the order changed to ∼−1. This maximum in activity was not expected, and no Pd-catalyzed nitrile hydrogenation results are reported in the literature showing this behavior. However, it is observed frequently in other hydrogenation and also in hydrogenolysis reactions using supported Pd catalysts where it is attributed to competitive adsorption [16–18,83–86]. Hydrogenolysis of simple alkanes over different supported catalysts all exhibited a negative order in H_2, and this was explained by the decreasing concentration of the dehydrogenated intermediate that undergoes C–C bond scission [20,87], although it was also speculated that competitive adsorption between H_2 and the hydrocarbons could play a role. To check whether competitive adsorption could indeed be the reason for our observation, we performed hydrogenation experiments at 20 and 30 bar with other $C_{BN,0}$ concentrations, viz., 1000 mol/m^3 and 300 mol/m^3. However, increasing or decreasing $C_{BN,0}$ did not have any influence on the *TOF* (Fig. 3a) and, as a consequence, this explanation is rejected.

4.2. The β-PdH phase

The sudden drop in activity around a pH_2 of 10 bar might be caused by the well-known formation of β-PdH. *Ex situ* XRD analysis of activated and non-activated catalysts showed remarkable changes of the Pd crystallite lattice parameters after activation at increased pH_2 (Fig. 5). The lattice constant of Pd increases by 2.0% after activation at 30 bar, which is attributed to the formation of the β-PdH phase. This observation is remarkable because the XRD patterns were measured *ex situ*, and probably all the hydrogen was already desorbed from the catalyst samples.

The conditions for a transformation of nanoscale Pd crystallites into β-PdH have been studied extensively. Typically, ∼1 bar H_2 is sufficient in the gas phase to transform supported nanoscale Pd crystallites into β-PdH at around 80 °C [30,88,89]. In the liquid phase, the critical value for pH_2 is expected to be much higher because the H_2 solubility in a liquid phase is an order of magnitude smaller than the H_2 concentration in the gas phase [35,41,90]. This corresponds with a pH_2 of ∼10 bar for liquid phase processes, nicely matching the pH_2 of 10 bar for the maximum in Fig. 3a. Note that the transformation of Pd into β-PdH is accelerated when the solvent is an alcohol compared to non-alcoholic solvents and water [91].

Under TPR conditions, the β-PdH phase is unstable above 80 °C as can be seen in Fig. 6, but it is striking that the expansion/distortion of the Pd lattice was still retained, as shown by *ex situ* XRD (see Fig. 5), after activation at 30 bar and a drying step performed at 120 °C in air. Several researchers observed the lattice distortion after the H_2 had been removed: only after annealing at 450 °C, the Pd atoms could be returned to their original position [25,92]. This also implies that the persistent expansion of the Pd lattice after activation of 30 bar could still have an effect on the catalyst performance during a hydrogenation experiment even if the β-PdH phase is somehow eliminated in between activation and hydrogenation.

When the catalyst precursor contains carbonaceous material or when a carbon support is used, carbon might incorporate in the Pd lattice and yield a solid solution in Pd (PdC) which could give similar shifts in reflections as β-PdH [26,93,94]. In our case, a PdC phase might be formed with the solvent (*i.e.* 2-propanol) as a carbon source. Formation of a PdC phase prohibits the formation of a β-PdH phase [65,93]. TPR is a useful technique for elucidating this point. If no β-PdH decomposition peak would be observed in the TPR profiles of the 10- and 30-bar activated catalysts then, the catalysts could have been contaminated by carbon soluble in the Pd lattice. However, we do see β-PdH decomposition peaks (Fig. 6) after the activation performed in 2-propanol, so it is concluded that no extensive PdC phase has been formed during the activation step. It should be noted that Teschner et al. observed that also a metastable PdC phase in the top few layers can be formed in the early stage of the reaction. This phase was only stable under reaction conditions during the gas-phase hydrogenation of acetylene at very low pH$_2$ (<0.13 bar) [95,96]. If the pH$_2$ is raised above a certain pressure, then this PdC surface phase disappears and a β-PdH phase is formed. Moreover, when trans-2-pentene is chosen as the reactant under similar reaction conditions, then no PdC phase is formed. Obviously, double bonds do not strongly fragment on the surface of Pd; hence, the C≡C triple bond is essential in forming a PdC surface phase. This is supported by DFT calculations, which shows that only for certain reactants, in combination with a Pd surface, a PdC surface phase can be formed [97–99]. Note that the morphology of the Pd catalyst is also important: decomposition of organic species takes place more efficiently on stepped than on flat surfaces [100]. Since our experiments were performed under completely different conditions and with other reactants than the ones used by Teschner et al. [95], we would argue against the formation of a metastable PdC surface phase in our experiments especially in view of the used pH$_2$.

4.3. Influence of β-PdH phase transformation on selectivity

The hydrogenation of BN over Pd/γ-Al$_2$O$_3$ in 2-propanol resulted in three products: BA, TOL, and DBA, at the investigated pH$_2$ range from 2.5 to 30 bar (Fig. 2). The production of BA dominated over the formation of TOL and DBA up to nearly full conversion of BN ($X_{BN} \sim 95\%$).

The highest Y_{BA} and S_{BA} achieved were above 90% and 95%, respectively, when a pH$_2$ was applied above 20 bar. This is an excellent result compared to other Pt-group catalysts and a good result compared to Ni catalysts (Table 1), considering that in this study no additives (*e.g.* NH$_3$) were used.

The maximum in catalyst activity at the threshold pH$_2$ of 10 bar is accompanied by sharp change in selectivities of TOL and DBA (Fig. 3e). As competitive adsorption is ruled out as explanation for the activity maximum at this pH$_2$, this cannot be the cause of this of this sharp selectivity change. Since the trends in selectivity and yield are similar, we will concentrate on the difference in selectivity in the following.

4.3.1. Influence of activation pressure

The performance of a catalyst activated at 10 bar and applied in a BN hydrogenation experiment at 30 bar resulted in the same performance as one activated at 30 bar and hydrogenation applied at 10 bar (Fig. 4a). Clearly, at 30 bar the β-PdH phase was formed, and this phase is stable during hydrogenation at lower pH$_2$. In agreement with this conclusion, activation at 2.5 bar and hydrogenation at 10 bar gave similar results as activation and hydrogenation at 10 bar. Apparently, if the pH$_2$ is high enough, then the Pd crystallites transform into a stable β-PdH phase that still determines the catalyst performance, even if the hydrogenation is carried out at a lower pH$_2$. If no stable β-PdH is formed during the activation step, *i.e.*, at pH$_2$ of 10 bar or lower, then the applied hydrogenation pH$_2$ determines the catalyst performance (Fig. 4b). So, a higher BA productivity can be achieved by applying an activation step above 10 bar prior to hydrogenation of BN at 10 bar compared to a standard experiment of both activation and hydrogenation at 10 bar.

4.3.2. Electronic interactions

The lattice expands and changes to the *d*-band of Pd occur upon transformation into the β-PdH phase [27,29–32,40,101–105]:

- Center of the *d*-band (ε_d) of β-PdH is shifted down compared to its Fermi level (E_f). The energy level of E_f does not change significantly when x (in β-PdH$_x$) is below 0.6 and is −5.22 eV for polycrystalline Pd. ε_d for Pd is 1.83 eV below E_f. ε_d for β-PdH$_{0.4}$ is ~2.2 eV below E_f. Catalytic activity is often related with the difference between ε_d and E_f: for a larger difference, the transition metal becomes less reactive [106–109].
- Width of the *d*-band of β-PdH$_{0.4}$ is ~15% narrower compared to Pd. A narrower *d*-band results in a decrease in Pauli repulsion. Weaker repulsive interactions increase the binding energy of adsorption with HOMO orbitals [110]. However, a spatially more extended *d*-band increases the propensity of rehybridization from π to di-σ coordination to overcome the larger repulsive interaction [111].

Thus, the lower BN hydrogenation activity above the threshold pH$_2$ of 10 bar can be caused by the lower ε_d (compared to E_f) and reduced width of the *d*-band of β-PdH compared to Pd.

Interaction of occupied (*e.g.* HOMO) and unoccupied molecular orbitals (*e.g.* LUMO) of an adsorbate with the broad *sp*-band of Pd is always attractive and causes broadening into resonances and a down shift in energy of these orbitals. Subsequently, hybridization between the *d*-band of Pd and the broadened molecular orbitals results in splitting of these orbitals, thereby forming bonding contributions at lower energies and antibonding ones at higher energies. The primary interactions during adsorption of BN are electron donation from occupied donative molecular orbitals of BN (π C≡N is the donating HOMO but also σ-donation from the lone pair on nitrogen is possible) to empty orbitals of Pd (*e.g.* d_z2 and *s*) and backdonation from occupied *d*-orbitals of Pd (*e.g.* $d_x2_{-y}2$) to the unoccupied acceptor molecular orbitals of BN (LUMO is π^* C≡N), similar to the Blyholder model for CO adsorption on transition metals [112]. However, donative interactions are mainly repulsive (Pauli repulsion) due to orthogonalization between occupied orbitals of BN and occupied *d*-orbitals of Pd [113]. These can only become attractive when donative orbital-derived antibonding orbitals are shifted up through E_f and become empty ('relieved repulsion') [114]: a higher energy level of the donative orbital results in more attraction and a stronger bond to the Pd surface. Backdonation is attractive if the energy level of the acceptor orbital (LUMO) is low enough in energy to interact with the *d*-band of Pd. Backdonation is always attractive because the antibonding part of the LUMO is too high in energy to be filled.

BN is the best electron acceptor of all the compounds involved in the hydrogenation of BN since it has the lowest LUMO (Table 3). The interaction of BN with Pd upon adsorption is mainly governed by electron backdonation of Pd to the LUMO of BN. This interaction is higher when the energy level of ε_d is higher and the *d*-band is wider as is the case for Pd compared to β-PdH. However, not only the strength of adsorption increases when increased backdonation occurs but the LUMO of BN is of antibonding character with respect to the C≡N bond and thus weakens this intramolecular bond and increases the reactivity of BN [114]. Additionally, the orientation mode changes from a more end-on to a more side-on adsorption orientation. Interaction of the *d*-band with the HOMO of BN will be mostly repulsive because this orbital is low in energy, thus

the bonding and antibonding orbitals from coupling to the *d*-band will mostly fall below E_f.

DBA and BA (and BIBA) are the best electron donors having the highest HOMOs (Table 3). In contrast to BN, the adsorption of BA and DBA on Pd is mainly governed by electron donation from their HOMO orbitals to unoccupied *d*-orbitals of Pd since the LUMOs of these amines have unfavorably high energy to sufficiently couple with the *d*-band of Pd. The HOMO of BA and DBA is localized on the lone pair of the nitrogen atom. The interaction is attractive since the HOMO of BA and DBA are sufficiently high-lying. This ensures that the antibonding orbitals originating from coupling of the *d*-band to the HOMO of BA (or DBA) are pushed above E_f and become empty. The interaction of the *d*-band of Pd with the HOMO of BA and DBA is increased upon a decrease in the width of the *d*-band (weaker repulsion) and a decrease in ε_d, as is the case for β-PdH. This is confirmed by TGA (Fig. 8). Operation above the threshold pH_2 results in more amine surface species than operation at below the threshold pH_2. Interaction of the *d*-band of Pd with the LUMO of the amines will be much less effective than with the LUMO of BN since the LUMO of the amines is significantly higher in energy (Table 3).

In conclusion, a lowering of ε_d and decrease in the width of the *d*-band upon the transformation into β-PdH will not only change the strength and orientation of adsorption to the surface of Pd but it will have different effects on BN and BA, thereby changing the adsorption ratio of BN/BA. The phase transformation of Pd results in a change in electronic and geometrical interactions with interacting species as schematically depicted in Fig. 9.

4.3.3. Adsorption of BN

The possible coordination states of adsorption of BN on Pd are shown in Fig. 10a [115–118]: end-on via σ-donation (I), side-on via σ-donation and π-backdonation (II), di-σ rehybridization of the C≡N group to sp^2 and sp^3 configuration (III, IV) and π-interactions with the phenyl and/or C≡N group (V). The extent of rehybridization is increased when backdonation increases and when the *d*-band is spatially more extended, as is the case for Pd compared to β-PdH. The DRIFT spectra shown in Fig. 7 give direct information on the modes of coordination of BN to Pd in catalysts used in hydrogenation at 10 and 20 bar. A blue shift in υ(C≡N) stretching compared to 2231.7 cm^{-1} of free BN implies strengthening of the C≡N bond and is mostly explained as end-on adsorption via electron donation from the nitrogen lone pair to acid sites on the γ-Al_2O_3 support [119]. Side-on adsorption, governed by electron backdonation, is not observed on Al_2O_3 supports [120,121]. So,

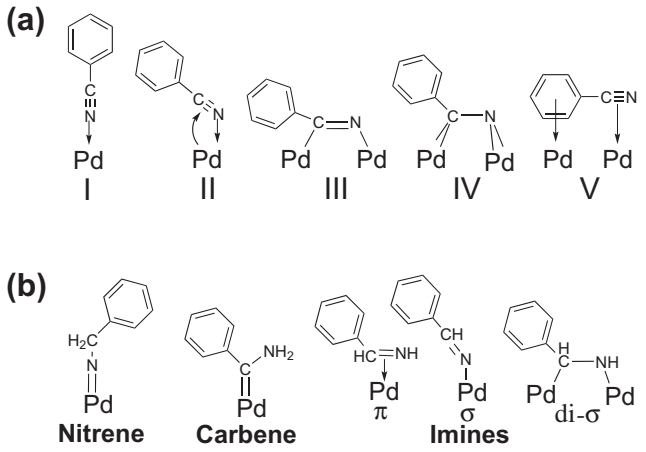

Fig. 10. (a) Possible adsorption modes of BN on Pd. (I) σ end-on adsorption; (II) side-on adsorption ($\sigma + \pi$); (III) di-σ rehybridized; (IV) further rehybridized; (V) π-interactions with phenyl and/or C≡N group. (b) Possible intermediate surface species after addition of two hydrogen atoms: nitrene, carbene, and three differently coordinated imines: σ, π, and di-σ.

the C≡N absorbance at wavenumbers below 2231.7 cm^{-1} are attributed to adsorption of BN on the Pd crystallites. However, both electron donation and backdonation occur when BN adsorbs on Pd crystallites, which causes a red shift of the C≡N stretching: electron backdonation results in a more side-on adsorption mode and a weaker C≡N bond [122]. The absorbance at 2230 cm^{-1} is attributed to an adsorption configuration, dominated by the nitrogen lone pair donation bond which is more end-on with relatively less backdonation (I), and the peak at 2165 cm^{-1} is attributed to a more side-on adsorption mode (II) with relatively more backdonation [117]. The differences in the 10- and 20-bar spectrum nicely supports the above reasoning: the absorbance intensity ratio of 2230–2165 cm^{-1} is much smaller for 10-bar hydrogenation than for 20-bar hydrogenation because of the transformation of Pd to β-PdH going from 10 to 20 bar. The larger electron backdonation of Pd compared to β-PdH results in a more side-on adsorption and a weaker C≡N bond.

4.3.4. The semi-hydrogenated intermediates

The most abundant semi-hydrogenated intermediate is BI, although it is not detected in the reaction mixture, because it reacts at the surface to BA without desorbing first [49]. As direct

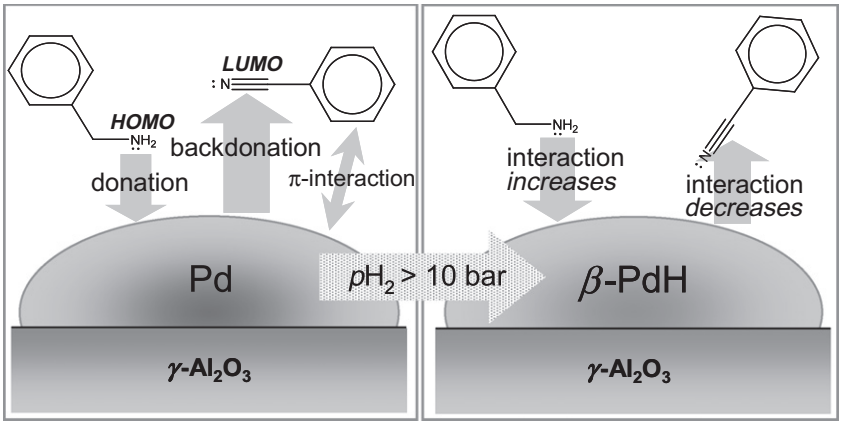

Fig. 9. Representation of major electron donation and electron withdrawing interactions between Pd, BN, and BA. Note the changing strength of interaction indicated by the arrow size, the changing orientation to the surface of BN, and the changing ratio of adsorption strengths BN/BA when Pd is transformed into β-PdH above the threshold pH_2 of 10 bar.

experimental evidence of BI is not reported in the literature, other possible surface intermediates might be present after partial hydrogenation of BN with two H atoms, such as nitrenes, carbenes, end-on, π-adsorbed and rehybridized imines (Fig. 10b) [2,123–128]. Recently, Schärringer et al. found experimental evidence of nitrene intermediates in the hydrogenation of $CD_3C{\equiv}N$ over Raney-Co [129]. In addition, interactions of the phenyl group of any of the intermediates with the Pd surface are possible [118]. For instance, the most stable calculated adsorption mode for BI on Pd(1 1 1) is via a combination of the C=N and phenyl group [130]. A priori, it is not clear which of the intermediates forms BA, DBA, and TOL, and speculations are based on work with aliphatic nitrile hydrogenation without considering hydrogenolysis. For the nitrene intermediate, the α-carbon is already saturated with hydrogen and thus not likely to be involved in one of the above-mentioned mechanisms, so nitrene intermediates will only form BA. In principle, the other intermediates can form BA, too, but can also undergo hydrogenolysis or condensation reactions. The most probable reaction pathways to BA, TOL, and DBA are shown in Fig. 11.

4.3.5. Hydrogenolysis to TOL

The main byproduct in the hydrogenation of BN was TOL, but above the threshold pH_2 a sharp decrease in S_{TOL} was observed as shown in Fig. 3e. From the discussion above, this can be understood from the formation of β-PdH with its relatively low backdonation to the adsorbates, thereby reducing the activation of the C≡N bond.

We speculate that a multicoordinated side-on adsorbed intermediate (*i.e.* σ/π-adsorbed imine), with interaction between the delocalized π-electrons of the phenyl ring and the Pd surface, is responsible for the direct hydrogenolysis of BN to TOL (11). The phenyl group in the vicinity of the C≡N group effectively lowers the activation energy toward TOL by stabilizing this adsorption mode internally by conjugation and by coordinating the phenyl group to the Pd surface [118]. This is seen more often in the literature: the hydrogenation of C=C and C=O bonds of aromatic molecules over Pd catalysts are activated by the presence of a phenyl group. This phenyl activation implies that the phenyl group adsorbs on active sites [131,132]. Carbene and nitrene species do not have a π-system, so the adsorbate will be more perpendicular orientated to the surface and hydrogenolysis to TOL is less probable.

Hydrogenolysis of BN to TOL is much more facile than hydrogenolysis of BA to TOL over the same supported Pd catalysts and conditions [133]. The rate of hydrogenolysis of BA ($C_{BA,0}$ = 520 - mol/m^3, pH_2 = 10 bar, and T = 80 °C) was 2.6 times lower than for BN, and the overall hydrogenation activity was 42 times lower. So, even though BA is an intermediate in the hydrogenolysis of BN to TOL, there are differences between the mechanism of BN and BA hydrogenolysis. BA will preferentially adsorb end-on with the lone pair of the nitrogen atom (highest HOMO). This explains the lower hydrogenolysis rate of BA compared to BN, since for hydrogenolysis of BA interaction is needed with both the phenyl and NH_2 group or with the phenyl ring only [134–137]. In Fig. 11, we propose a π-benzyl complex as intermediate toward breakage of the C–N bond in BA. An alternative mechanism is that

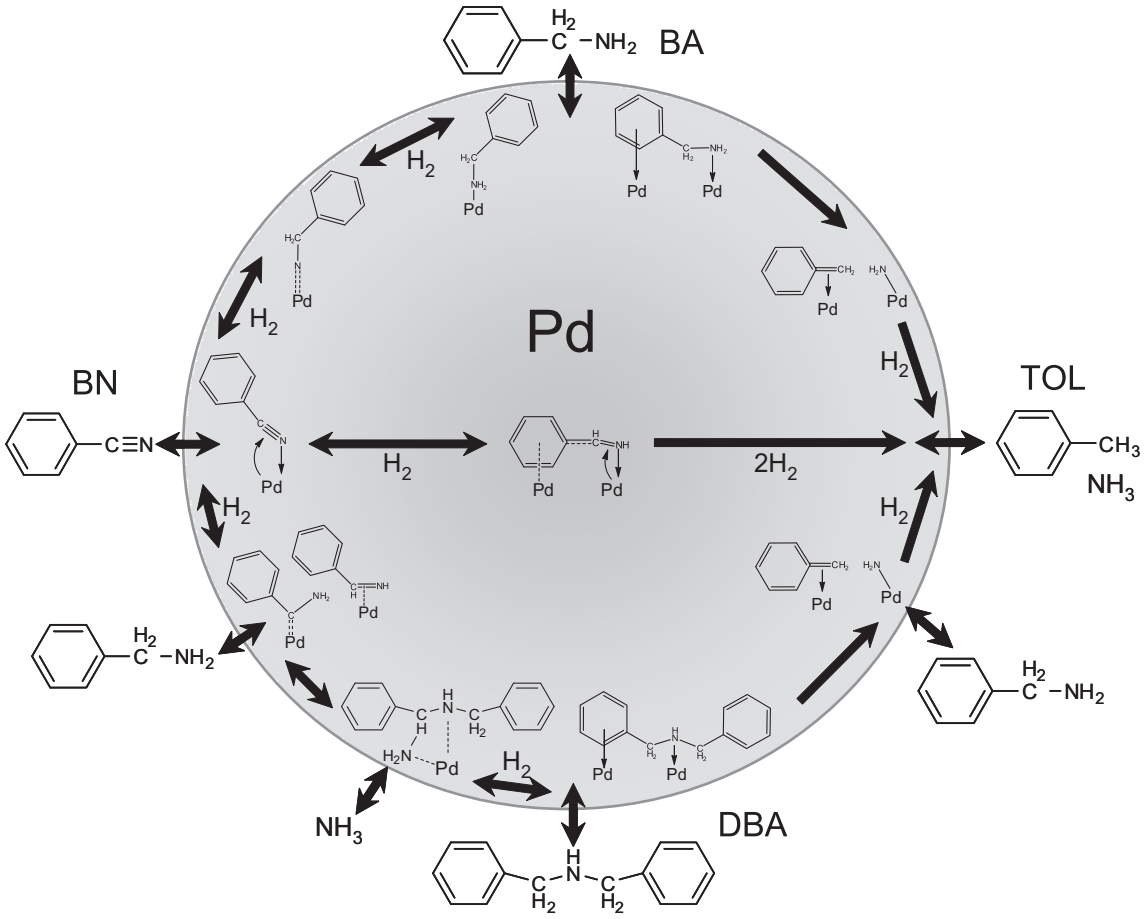

Fig. 11. Reaction scheme of the hydrogenation of BN showing the reaction pathways toward the products BA, DBA, and TOL. This scheme shows which semi-hydrogenated intermediates are most probable to form BA, DBA, and TOL and shows the multiple pathways to TOL: via BN (direct hydrogenolysis) and via readsorbed BA and DBA (BA and DBA hydrogenolysis). Note that all semi-hydrogenated intermediates (carbene, imine and nitrene) can form BA (not indicated). The transformation of Pd to β-PdH above the threshold pH_2 decreases the hydrogenolysis to TOL and increases the condensation to DBA.

BA first partially dehydrogenates to a hydrogen-deficient intermediate (*i.e.* di-σ rehybridized semi-hydrogenated intermediate) followed by the breakage of the C–N bond, similar to that proposed for the hydrogenolysis of methylamines and alkanes [86,138,139].

Note that we propose that DBA forms TOL and BA via a similar mechanism. Furthermore, TOL is formed immediately after the reaction was started (*e.g.* Fig. 2a), which is additional evidence for a direct hydrogenolysis route of BN to TOL via surface intermediates without intermediates (*i.e.* BA and DBA) desorption [140,141]. Hydrogenation of an equimolar mixture of BN and BA (pH_2 = 10 bar and T = 80 °C) gave 1.7 times lower overall hydrogenation activity and 3.4 times lower hydrogenolysis rate resulting in a higher S_{BA}. This shows that BN and BA adsorb competitively on the same active sites but BN adsorbs stronger than BA. Still, BA blocks active sites for BN hydrogenolysis by reducing the probability for multicoordinated side-on adsorption. This, together with the slower BA hydrogenolysis rate compared to BN hydrogenolysis, accounts for the lower S_{TOL}.

4.3.6. Condensation to DBA

Secondary amine formation is usually explained by the nucleophilic attack of a primary amine with the lone pair on the nitrogen atom on an electrophilic carbon atom of semi-hydrogenated intermediate (*i.e.* imine, carbene, and rehybridized species). The initially *s*-shaped curve of DBA formation (Fig. 2a) is typical for a consecutive reaction, *i.e.*, the bimolecular reaction between a semi-hydrogenated intermediate and BA. Carbene and to a lesser extent imine intermediates have the highest probability to form DBA because of the unsaturated electrophilic carbon atom (Fig. 11). BIBA is assumed to be the intermediate, although it has never been observed [142].

The low S_{DBA}, over the whole investigated pH_2 range, can be explained by the low nucleophilicity of BA, caused by conjugation effects that delocalize the electron density of nitrogen. It is striking that DBA is the main product when BN is hydrogenated over supported Pt catalysts (Table 1). Clearly, the catalyst plays a crucial role in determining selectivity. The difference between Pt and Pd could be explained as follows. Compared to Pt (with a lower E_f, a lower ε_d, and a more extended *d*-band compared to Pd), the Pd surface is populated with semi-hydrogenated intermediates that are much less susceptible to condensation, *i.e.*, nitrenes, and the subsequent desorption of BA is easier. Furthermore, the fast rate of hydrogenation to BA of these intermediates compared to the slow formation from BN result in a low surface coverage.

TOL is the main byproduct: Y_{TOL} is always higher than Y_{DBA} (Fig. 3c). However, above the threshold pH_2, S_{DBA} becomes higher than S_{TOL} (Fig. 3e). This is attributed to an increased amount of BA on the surface of β-PdH compared to Pd because of the decreased Pauli repulsion and the lower ε_d. The decreased S_{TOL} implies also a lower NH_3 content (NH_3 suppresses the condensation to DBA [4]). Moreover, the decreased electron backdonation of β-PdH to an intermediate results in a more electropositive carbon atom, which will be more susceptible to a nucleophilic attack by BA to DBA.

5. Conclusions

The influence of hydrogen pressure on the semi-batch hydrogenation of benzonitrile to benzylamine over a γ-alumina-supported palladium catalyst in 2-propanol was investigated to explain the maximum in activity and the selectivity change around a certain hydrogen threshold pressure. An important message of this study for practical operation of selective hydrogenations over palladium catalysts is the careful selection of the operational and activation pressure. An optimum must be sought between activity and selectivity and the active-phase structure of palladium. The changed electronic properties of palladium may result in drastic changes in adsorption strengths and modes and consequently in activity and selectivity.

- The main product was benzylamine over the whole investigated pressure range. Byproducts were toluene and dibenzylamine. A yield of benzylamine up to 90% was reached without any additives.
- Palladium completely transforms into palladium β-hydride above the threshold hydrogen pressure of 10 bar, identified by *ex situ* XRD. The expansion of the palladium lattice caused by hydrogen incorporation was irreversible at the applied conditions.
- The activation pressure influences the performance of the catalyst if the pressure is high enough to transform palladium into palladium β-hydride during activation. This palladium β-hydride, which is formed during activation, is then stable during hydrogenation at lower hydrogen pressure and results in equal activity and selectivities as hydrogenation at higher hydrogen pressures.
- The palladium β-hydride phase has a lower benzonitrile hydrogenation activity attributed to electronic modifications of the *d*-band of palladium upon the transformation to palladium that decreases the electron backdonation to benzonitrile, resulting in a less-activated nitrile group.
- The changed electronic properties of palladium upon the formation of the palladium β-hydride modify the modes and strength of benzonitrile adsorption, thereby influencing the type and amount of intermediates, resulting in a changed selectivity:
    - Hydrogenolysis to toluene is decreased above the threshold pressure.
    - Condensation to dibenzylamine is increased above the threshold pressure.
- Toluene can be formed directly from benzonitrile and indirectly from readsorbed benzylamine and dibenzylamine. Both direct and indirect hydrogenolysis reactions proceed via different pathways: the rate of hydrogenolysis of benzylamine is slower than that of benzonitrile. Interaction via the π-electrons of the aromatic ring is a prerequisite for facile hydrogenolysis. For palladium β-hydride, this interaction is less than for palladium.
- The formation of palladium β-hydride resulted in a higher amount of benzylamine on the surface due to the higher adsorption strength and a decreased benzylamine hydrogenolysis, explaining a higher degree of condensation to dibenzylamine.
- The condensation to dibenzylamine is further enhanced by the lower production of inhibiting ammonia and by the decreased electron backdonation, yielding surface intermediates that are more susceptible to an attack from nucleophiles.

Acknowledgments

Ferdinand C. Grozema of the Opto-electronic Materials section of the Delft University of Technology is acknowledged for fruitful discussions.

Appendix A. Supplementary material

Supplementary material regarding mass transport limitations and details of the used characterization techniques can be found, in the online version, at doi:10.1016/j.jcat.2010.06.013.

References

[1] S. Nishimura, Handbook of Heterogeneous Catalytic Hydrogenation for Organic Synthesis, Wiley-VCH, New York, 2001. pp. 254–285.

[2] C. De Bellefon, P. Fouilloux, Catal. Rev. Sci. Eng. 36 (1994) 459–506.
[3] J. Volf, J. Pasek, in: L. Cerveny (Ed.), Catalytic Hydrogenation, Elsevier, Amsterdam, 1986, p. 105.
[4] S. Gomez, J.A. Peters, T. Maschmeyer, Adv. Synth. Catal. 344 (2002) 1037–1057.
[5] P. Sabatier, J.R. Senderens, C.R. Hebd, Seances Acad. Sci. 140 (1905) 482.
[6] G. Mignonac, C.R. Hebd, Seances Acad. Sci. 171 (1920) 114–117.
[7] J. von Braun, G. Blessing, F. Zobel, Chem. Ber. 36 (1923) 1988–2001.
[8] K. Kindler, F. Hesse, Arch. Pharm. 27 (1933) 439–445.
[9] H. Greenfield, Ind. Eng. Chem. Prod. Res. Dev. 15 (1976) 156–158.
[10] Y. Huang, W.M.H. Sachtler, J. Catal. 184 (1999) 247–261.
[11] P. Rylander, Catalytic Hydrogenation in Organic Syntheses, 1979, p. 138.
[12] P.N. Rylander, L. Hasbrouck, I. Karpenko, Ann. NY Acad. Sci. 214 (1973) 100–109.
[13] P.N. Rylander, J.G. Kaplan, US Patent 3117,162, 1964.
[14] S.P. Bawane, S.B. Sawant, Chem. Eng. J. (Lausanne) 103 (2004) 13–19.
[15] L. Hegedus, T. Máthé, Appl. Catal. A 296 (2005) 209–215.
[16] H. Bernas, A. Taskinen, J. Wärnå, D.Y. Murzin, J. Mol. Catal. A: Chem. 306 (2009) 33–39.
[17] V. Dubois, G. Jannes, J.L. Dallons, A. Van Gysel, in: J.R. Kosak, T.A. Johnson (Eds.), Catalysis of Organic Reactions, Marcel Dekker Inc., 1994, p. 1.
[18] E.V. Skakunova, M.M. Ermilova, V.M. Gryaznov, Izv. Akad. Nauk Gruz. SSR, Ser. Khim (1988) 986–991.
[19] J.H. Sinfelt, Catal. Lett. 9 (1991) 159–171.
[20] J.H. Sinfelt, Cat. Rev. 3 (1969) 175–205.
[21] J.H. Sinfelt, Adv. Catal. 23 (1973) 91–119.
[22] J.H. Sinfelt, J.L. Carter, D.J.C. Yates, J. Catal. 24 (1972) 283–296.
[23] J.H. Sinfelt, D.J.C. Yates, J. Catal. 8 (1967) 82–90.
[24] T. Graham, Philos. Trans. Roy. Soc. 156 (1866) 399–439.
[25] L.L. Jewell, B.H. Davis, Appl. Catal. A 310 (2006) 1–15.
[26] N.K. Nag, J. Phys. Chem. B 105 (2001) 5945–5949.
[27] R.J. Davis, S.M. Landry, J.A. Horsley, M. Boudart, Phys. Rev. B 39 (1989) 10580–10583.
[28] K. Christmann, in: Z. Paal, P.G. Menon (Eds.), Hydrogen Effects in Catalysis. Fundamentals and Practical Applications, Marcel Dekker Inc., New York, 1988, p. 44.
[29] I.P. Chernov, Y.M. Koroteev, V.M. Silkin, Y.I. Tyurin, Dokl. Phys. 53 (2008) 318–322.
[30] M. Yamauchi, R. Ikeda, H. Kitagawa, M. Takata, J. Phys. Chem. C 112 (2008) 3294–3299.
[31] C.T. Chan, S.G. Louie, Phys. Rev. B 27 (1983) 3325–3337.
[32] J.S. Faulkner, Phys. Rev. B 13 (1976) 2391–2397.
[33] F. Pinna, M. Signoretto, G. Strukul, S. Polizzi, N. Pernicone, React. Kinet. Catal. Lett. 60 (1997) 9–13.
[34] M. Boudart, H.S. Hwang, J. Catal. 39 (1975) 44–52.
[35] A.J. Bird, D.T. Thompson, in: W.H. Jones (Ed.), Catalysis in Organic Syntheses, Academic Press, New York, 1980, p. 61.
[36] A. Valcarcel, F. Morfin, L. Piccolo, J. Catal. 263 (2009) 315–320.
[37] D. Teschner, J. Borsodi, A. Wootsch, Z. Revay, M. Havecker, A. Knop-Gericke, S.D. Jackson, R. Schlogl, Science 320 (2008) 86–89.
[38] D. Teschner, Z. Révay, J. Borsodi, M. Hävecker, A. Knop-Gericke, R. Schlögl, D. Milroy, S.D. Jackson, D. Torres, P. Sautet, Angew. Chem. 120 (2008) 9414–9418.
[39] F. Studt, F. Abild-Pedersen, T. Bligaard, Rasmus, Z. Sørensen, Claus, H. Christensen, Jens K. Nørskov, Angew. Chem. Int. Ed. 47 (2008) 9299–9302.
[40] M.P. Jigato, B. Coussens, D.A. King, J. Chem. Phys. 118 (2003) 5623–5634.
[41] Á. Mastalir, Z. Király, F. Berger, Appl. Catal. A 269 (2004) 161–168.
[42] G. Carturan, G. Facchin, G. Cocco, S. Enzo, G. Navazio, J. Catal. 76 (1982) 405–417.
[43] H. Greenfield, and R.S. Sekellick, US Patent 3923,891, 1975.
[44] O.G. Degischer, F. Roessler, P. Rys, Chem. Ind.: Catal Org. React. 82 (2001) 241–254.
[45] Y.M. Lopez-De Jesus, A. Vicente, G. Lafaye, P. Marecot, C.T. Williams, J. Phys. Chem. C 112 (2008) 13837–13845.
[46] T. Fuchigami, S. Takamizawa, and N. Wakasa, US Patent 6476,267 B1, 2002.
[47] M.B. Dines, P.M. DiGiacomo, and K.P. Callahan, US Patent 4384,981, 1983.
[48] D. Ostgard, M. Berweiler, and S. Roder, US Patent 0173676 A1, 2002.
[49] D.J. Ostgard, Spec. Chem. Mag. 28 (2008) 28–31.
[50] K. Hata, K. Watanabe, Bull. Chem. Soc. Jpn. 32 (1959) 861–867.
[51] S. Galvagno, A. Donato, G. Neri, R. Pietropaolo, J. Mol. Catal. 58 (1990) 215–225.
[52] R.A. Plunkett, J.L. Neff, and T.A. Bemish, US Patent 4163,025, 1979.
[53] S. Gobolos, N. Mahata, I. Borbath, M. Hegedus, J.L. Margitfalvi, React. Kinet. Catal. Lett. 74 (2001) 345–352.
[54] O. Domínguez-Quintero, S. Martínez, Y. Henríquez, L. D'Ornelas, H. Krentzien, J. Osuna, J. Mol. Catal. A: Chem. 197 (2003) 185–191.
[55] H. Paul, S. Basu, S. Bhaduri, G.K. Lahiri, J. Organomet. Chem. 689 (2004) 309–316.
[56] A.W. Heinen, J.A. Peters, H. Van Bekkum, Eur. J. Org. Chem. (2000) 2501–2506.
[57] S. Enthaler, K. Junge, D. Addis, G. Erre, M. Beller, ChemSusChem 1 (2008) 1006–1010.
[58] C. Amorim, M.A. Keane, J. Colloid Interface Sci. 322 (2008) 196–208.
[59] G. Fagherazzi, A. Benedetti, S. Polizzi, A. Mario, F. Pinna, M. Signoretto, N. Pernicone, Catal. Lett. 32 (1995) 293–303.
[60] J. Sa, G.D. Arteaga, R.A. Daley, J. Bernardi, J.A. Anderson, J. Phys. Chem. B 110 (2006) 17090–17095.
[61] S. Huang, C. Huang, B. Chang, C. Yeh, J. Phys. Chem. B 110 (2006) 21783–21787.
[62] A.R. Denton, N.W. Ashcroft, Phys. Rev. A 43 (1991) 3161–3164.
[63] E.F. Skelton, P.L. Hagans, S.B. Qadri, D.D. Dominguez, A.C. Ehrlich, J.Z. Hu, Phys. Rev. B 58 (1998) 14775–14779.
[64] Z. Kaszkur, J. Appl. Crystallogr. 33 (2000) 1262–1270.
[65] C.M. Mendez, H. Olivero, D.E. Damiani, M.A. Volpe, Appl. Catal. B 84 (2008) 156–161.
[66] N.S. Babu, N. Lingaiah, R. Gopinath, P.S. Sankar Reddy, P.S. Sai Prasad, J. Phys. Chem. C 111 (2007) 6447–6453.
[67] J. Panpranot, K. Pattamakomsan, P. Praserthdam, J.G. Goodwin, Ind. Eng. Chem. Res. 43 (2004) 6014–6020.
[68] J. Panpranot, O. Tangjitwattakorn, P. Praserthdam, J.G. Goodwin Jr., Appl. Catal. A 292 (2005) 322–327.
[69] H. Lieske, J. Voelter, J. Phys. Chem. 89 (1985) 1841–1842.
[70] M. Gurrath, T. Kuretzky, H.P. Boehm, L.B. Okhlopkova, A.S. Lisitsyn, V.A. Likholobov, Carbon 38 (2000) 1241–1255.
[71] B. Wen, Q. Sun, W.M.H. Sachtler, J. Catal. 204 (2001) 314–323.
[72] M. Bonarowska, J. Pielaszek, W. Juszczyk, Z. Karpinski, J. Catal. 195 (2000) 304–315.
[73] H. Knoezinger, H. Krietenbrink, J. Chem. Soc. Faraday Trans. 71 (1975) 2421–2430.
[74] R.A. Nyquist, Appl. Spectrosc. 44 (1990) 1405–1407.
[75] H. Sato, Y. Kusumoto, S. Arase, M. Suenaga, S. Kammura, J. Phys. Chem. 82 (1978) 66–68.
[76] P. Hirva, T.A. Pakkanen, Surf. Sci. 277 (1992) 389–394.
[77] M. Skotak, Z. Karpinski, W. Juszczyk, J. Pielaszek, L. Kepinski, D.V. Kazachkin, V.I. Kovalchuk, J.L. d'Itri, J. Catal. 227 (2004) 11–25.
[78] A. Quintanilla, J.J.W. Bakker, M.T. Kreutzer, J.A. Moulijn, F. Kapteijn, J. Catal. 257 (2008) 55–63.
[79] W.J. Kim, E.W. Shin, J.H. Kang, S.H. Moon, Appl. Catal. A 251 (2003) 305–313.
[80] P. Marécot, A. Akhachane, J. Barbier, Catal. Lett. 36 (1996) 37–39.
[81] J.-W. Park, Y.-M. Chung, Y.-W. Suh, H.-K. Rhee, Catal. Today 93–95 (2004) 445–450.
[82] M.R. Othman, I.S. Sahadan, Micropor. Mesopor. Mater. 91 (2006) 145–150.
[83] F. Figueras, B. Coq, J. Mol. Catal. A: Chem. 173 (2001) 223–230.
[84] G. Meitzner, W.J. Mykytka, J.H. Sinfelt, J. Catal. 98 (1986) 513–521.
[85] G. Meitzner, W.J. Mykytka, J.H. Sinfelt, Catal. Lett. 37 (1996) 137–141.
[86] G. Meitzner, W.J. Mykytka, J.H. Sinfelt, Catal. Lett. 32 (1995) 335–344.
[87] L. Guczi, A. Sarkany, P. Tetenyi, J. Chem. Soc. Faraday Trans. 70 (1974) 1971–1981.
[88] A. Pundt, R. Kirchheim, Annu. Rev. Mater. Res. 36 (2006) 555–608.
[89] A. Pundt, M. Suleiman, C. Bähtz, M.T. Reetz, R. Kirchheim, N.M. Jisrawi, Mater. Sci. Eng. B 108 (2004) 19–23.
[90] P.C. Aben, J. Catal. 10 (1968) 224–229.
[91] I.T. Caga, E. Shutt, J.M. Winterbottom, J. Catal. 44 (1976) 271–280.
[92] E.A. Owen, J.I. Jones, Proc. Phys. Soc. 49 (1937) 603–610.
[93] S.B. Ziemecki, G.A. Jones, J. Catal. 95 (1985) 621–622.
[94] E.J.A.X. van de Sandt, A. Wiersma, M. Makkee, H. van Bekkum, J.A. Moulijn, Appl. Catal. A 155 (1997) 59–73.
[95] D. Teschner, E. Vass, M. Havecker, S. Zafeiratos, P. Schnorch, H. Sauer, A. Knop-Gericke, R. Schloegl, M. Chamam, A. Wootsch, A.S. Canning, J.J. Gamman, S.D. Jackson, J. McGregor, L.F. Gladden, J. Catal. 242 (2006) 26–37.
[96] D. Teschner, J. Borsodi, Z. Kis, L. Szentmiklosi, Z. Revay, A. Knop-Gericke, R. Schlogl, D. Torres, P. Sautet, J. Phys. Chem. C 114 (2010) 2293–2299.
[97] N. Seriani, F. Mittendorfer, G. Kresse, J. Chem. Phys. 132 (2010) 1–8.
[98] P. Sautet, F. Cinquini, ChemCatChem 2 (2010) 636–639.
[99] M. García-Mota, B. Bridier, J. Pérez-Ramírez, N. López, J. Catal. (2010), doi:10.1016/j.jcat.2010.1004.1018.
[100] J. Andersin, N. Lopez, K. Honkala, J. Phys. Chem. C 113 (2009) 8278–8286.
[101] D.A. Papaconstantopoulos, B.M. Klein, J.S. Faulkner, L.L. Boyer, Phys. Rev. B 18 (1978) 2784–2791.
[102] S. Mizusaki, N. Hiraoka, I. Yamamoto, M. Itou, Y. Sakurai, M. Yamaguchi, J. Phys. Soc. Jpn. 72 (2003) 1145–1151.
[103] D.E. Eastman, J.K. Cashion, A.C. Switendick, Phys. Rev. Lett. 27 (1971) 35.
[104] W. Jaworski, J. Phys. F: Met. Phys. 17 (1987) 373–381.
[105] M. Gupta, A.J. Freeman, Phys. Rev. B 17 (1978) 3029.
[106] B. Hammer, J.K. Nørskov, Surf. Sci. 343 (1995) 211–220.
[107] B. Hammer, J.K. Nørskov, Nature 376 (1995) 238–240.
[108] A. Ruban, B. Hammer, P. Stoltze, H.L. Skriver, J.K. Nørskov, J. Mol. Catal. A: Chem. 115 (1997) 421–429.
[109] P. Liu, J.K. Nørskov, Phys. Chem. Chem. Phys. 3 (2001) 3814–3818.
[110] P. Gallezot, D. Richard, Catal. Rev. Sci. Eng. 40 (1998) 81–126.
[111] B.A. Averill, I.M.C.M. Rietjens, P.W.N.M. Van Leeuwen, R.A. Van Santen, Stud. Surf. Sci. Catal. 123 (1999) 109–208.
[112] G. Blyholder, J. Phys. Chem. 68 (1964) 2772–2777.
[113] T. Bligaard, J.K. Nørskov, Chemical Bonding at Surfaces and Interfaces, Elsevier, Amsterdam, 2008. p. 255.
[114] I. Chorkendorff, J.W. Niemantsverdriet, Concepts of Modern Catalysis and Kinetics, WILEY-VCH, Weinheim, 2003. p. 215.
[115] K. Kishi, F. Kikui, S. Ikeda, Surf. Sci. 99 (1980) 405–418.
[116] T. Nakayama, K. Inamura, Y. Inoue, S. Ikeda, K. Kishi, Surf. Sci. 179 (1987) 47–58.
[117] O. Oranskaya, I. Semenskaya, V. Filimonov, React. Kinet. Catal. Lett. 5 (1976) 135–139.

[118] S. Zou, C.T. Williams, E.K.Y. Chen, M.J. Weaver, J. Phys. Chem. B 102 (1998) 9039–9049.
[119] K.F. Purcell, R.S. Drago, J. Am. Chem. Soc. 88 (1966) 919–924.
[120] E. Paukstis, E.N. Yurchenko, Usp. Khim. 52 (1983) 426–454.
[121] O.M. Oranskaya, V.N. Filimonov, E.Y. Shmulyakovskii, Vopr. Mol. Spektrosk. (1974) 195–198.
[122] J. Raskó, J. Kiss, Appl. Catal. A. 298 (2006) 115–126.
[123] A. Chojecki, H. Jobic, A. Jentys, T.E. Müller, J.A. Lercher, Catal. Lett. 97 (2004) 155–162.
[124] A. Chojecki, M. Veprek-Heijman, T.E. Müller, P. Schärringer, S. Veprek, J.A. Lercher, J. Catal. 245 (2007) 237–248.
[125] B. Coq, D. Tichit, S. Ribet, J. Catal. 189 (2000) 117–128.
[126] B. Bigot, F. Delbecq, A. Milet, V.-H. Peuch, J. Catal. 159 (1996) 383–393.
[127] P. Schärringer, T.E. Müller, J.A. Lercher, J. Catal. 253 (2008) 167–179.
[128] J. Krupka, J. Patera, Appl. Catal. A 330 (2007) 96–107.
[129] P. Schärringer, T.E. Müller, A. Jentys, J.A. Lercher, J. Catal. 263 (2009) 34–41.
[130] L. Hegedus, T. Máthé, T. Kárpáti, Appl. Catal. A 349 (2008) 40–45.
[131] J. Jenck, J.-E. Germain, J. Catal. 65 (1980) 141–149.
[132] J.L. Dallons, G. Jannes, B. Delmon, Catal. Today 5 (1989) 257–264.
[133] W.F. Maier, P. Grubmüller, I. Thies, P.M. Stein, M.A. McKervey, P.v.R. Schleyer, Angew. Chem. Int. Ed. 18 (1979) 939–940.
[134] S. Mitsui, Y. Sugi, Tetrahedron Lett. 10 (1969) 1291–1294.
[135] Y. Sugi, S. Mitsui, Tetrahedron 29 (1973) 2041–2045.
[136] C.Ó. Murchú, Tetrahedron Lett. 10 (1969) 3231–3234.
[137] K. Ikedate, S. Suzuki, Nippon Kagaku Kaishi (1975) 234–241.
[138] D.F. Johnson, Y. Wang, J.E. Parmeter, M.M. Hills, W.H. Weinberg, J. Am. Chem. Soc. 114 (1992) 4279–4290.
[139] J.R. Anderson, N.J. Clark, J. Catal. 5 (1966) 250–263.
[140] M. Jian, F. Kapteijn, R. Prins, J. Catal. 168 (1997) 491–500.
[141] T. Vergunst, F. Kapteijn, J.A. Moulijn, Catal. Today 66 (2001) 381–387.
[142] Y. Huang, W.M.H. Sachtler, Appl. Catal. A 182 (1999) 365–378.